Chemical composition and source attribution of submicron aerosol particles in the summertime Arctic lower troposphere

Franziska Köllner[1,a], Johannes Schneider[1], Megan D. Willis[2,b], Hannes Schulz[3], Daniel Kunkel[4], Heiko Bozem[4], Peter Hoor[4], Thomas Klimach[1], Frank Helleis[1], Julia Burkart[2,c], W. Richard Leaitch[5], Amir A. Aliabadi[5,d], Jonathan P. D. Abbatt[2], Andreas B. Herber[3], and Stephan Borrmann[4,1]

[1]Max Planck Institute for Chemistry, Mainz, Germany
[2]Department of Chemistry, University of Toronto, Canada
[3]Alfred Wegener Institute for Polar and Marine Research, Bremerhaven, Germany
[4]Institute for Atmospheric Physics, Johannes Gutenberg University Mainz, Germany
[5]Environment and Climate Change Canada, Toronto, Canada
[a]now at: Institute for Atmospheric Physics, Johannes Gutenberg University Mainz, Germany
[b]now at: Lawrence Berkeley National Laboratory, Chemical Sciences Division, Berkeley, USA
[c]now at: Aerosol Physics and Environmental Physics, University of Vienna, Austria
[d]now at: Environmental Engineering Program, University of Guelph, Guelph, Canada

Correspondence: Franziska Köllner (f.koellner@mpic.de)

Abstract. We use airborne measurements of aerosol particle composition to demonstrate the strong contrast between particle sources and composition within and above the summertime Arctic boundary layer. In-situ measurements from two complementary aerosol mass spectrometers, the ALABAMA and the HR-ToF-AMS, with black carbon measurements from an SP2 are presented. Particle composition analysis was complemented by trace gas measurements, satellite data, and air mass history modeling to attribute particle properties to particle origin and air mass source regions. Particle composition above the summertime Arctic boundary layer was dominated by chemically aged particles, containing elemental carbon, nitrate, ammonium, sulfate, and organic matter. From our analysis, we conclude that the presence of these particles was driven by transport of aerosol and precursor gases from mid-latitudes to Arctic regions. Particularly, elevated concentrations of nitrate, ammonium, and organic matter coincided with time spent over vegetation fires in northern Canada. In parallel, those particles were largely present in high CO environments ($> 90\,\mathrm{ppb_v}$). Additionally, we observed that the organic-to-sulfate ratio was enhanced with increasing influence from these fires. Besides vegetation fires, particle sources in mid-latitudes further include anthropogenic emissions in Europe, North America, and East Asia. The presence of particles in the Arctic lower free troposphere correlated with time spent over populated and industrial areas in these regions. Further, the size distribution of free tropospheric particles containing elemental carbon and nitrate was shifter to larger diameters compared to particles present within the boundary layer. Moreover, our analysis suggests that organic matter when present in the Arctic free troposphere can partly be identified as low-molecular weight dicarboxylic acids (oxalic, malonic, and succinic acid). Particles containing dicarboxylic acids were largely present when the residence time of air masses outside Arctic regions was high. In contrast, particle composition within the marine boundary layer was largely driven by Arctic regional processes. Air mass history modeling demonstrated that

alongside primary sea spray particles, marine-biogenic sources contributed to secondary aerosol formation by trimethylamine,
20   methanesulfonic acid, sulfate, and other organic species.

1   Introduction

In the face of rapid climate changes in the Arctic (IPCC, 2014; IPPC, 2018), polar research has intensified to understand the
key processes driving these changes and their effects on the Arctic environment (e.g., Serreze and Francis, 2006; Serreze et al.,
25   2009; Flanner et al., 2011; Stroeve et al., 2012; Pithan and Mauritsen, 2014). Observed amplified Arctic warming in recent
decades and coupled rapid sea ice retreat are attributed to various causes, including increases in greenhouse gases and local
feedback mechanisms, such as the snow/ice-albedo feedback (e.g., Curry et al., 1995; Holland and Bitz, 2003; Serreze and
Barry, 2011; Flanner et al., 2011; Stroeve et al., 2012; Pithan and Mauritsen, 2014; Law et al., 2014; Arnold et al., 2016).
However, one important aspect concerning the Arctic climate system pertains to the coupling between aerosol, clouds, and
30   radiation. Interaction between aerosol particles, clouds, and radiation strongly depends on number, size, and chemical compo-
sition of the aerosol particles (e.g., Haywood and Boucher, 2000; Boucher et al., 2013), which are in turn influenced by particle
sources, formation, and atmospheric processing.

In Arctic summer, organic matter significantly contributes to submicron aerosol mass (e.g., Schmale et al., 2011; Chang et al.,
2011; Lathem et al., 2013; Breider et al., 2014; Willis et al., 2017; Leaitch et al., 2018; Lange et al., 2018; Tremblay et al.,
35   2019). Organic aerosol encompasses a large variety of chemical compounds that vary significantly across Arctic sites, ow-
ing to differences in sources and chemical processing (e.g., Shaw et al., 2010; Fu et al., 2013; Hansen et al., 2014; Leaitch
et al., 2018). Boreal fires and to a lesser extent anthropogenic activities in North America and northern Eurasia can strongly
influence the organic aerosol burden in the summer Arctic free troposphere (FT) (Hirdman et al., 2010; Schmale et al., 2011;
Lathem et al., 2013; Breider et al., 2014). Whereas in the summertime Arctic boundary layer (BL), organic matter can also
40   be influenced by both primary emissions and secondary chemical processes from Arctic marine and terrestrial sources (e.g.,
Willis et al., 2016, 2017; Köllner et al., 2017; Croft et al., 2019). Sources and identities of secondary organic aerosol (SOA)
are poorly characterized (Willis et al., 2018). However, tracers of SOA, including a variety of dicarboxylic acids (DCA), such
as oxalic, malonic, and succinic acid, have been detected at Arctic sites (e.g., Kawamura et al., 1996; Kerminen et al., 1999;
Fu et al., 2009; Kawamura et al., 2012; Fu et al., 2013; Hansen et al., 2014). Several studies demonstrated that particulate
45   DCA are less abundant in summer than in spring, driven by diminished long range transport of precursors and efficient aerosol
wet removal. In parallel, natural regional sources of DCA become more important as sea ice melts and biological productivity
increases (e.g., Kawamura et al., 1996; Kerminen et al., 1999; Kawamura et al., 2010, 2012).

Sulfate concentrations in the summertime Arctic FT are largely influenced by anthropogenic sources in northern Eurasia, North
America, and East Asia (Shindell et al., 2008; Hirdman et al., 2010; Kuhn et al., 2010; Bourgeois and Bey, 2011; Schmale

50   et al., 2011; Breider et al., 2014; Yang et al., 2018; Sobhani et al., 2018). While in the summertime Arctic BL, sulfate concentrations are dominated by emissions of dimethylsulfide from Arctic marine sources (e.g., Breider et al., 2014; Yang et al., 2018). However, sulfur emissions from volcanoes or Smoking Hills in northern Canada may impact episodically Arctic surface concentrations (e.g., Radke and Hobbs, 1989; Breider et al., 2014; Leaitch et al., 2018). In contrast, the summertime Arctic black carbon (BC) burden is mainly controlled by vegetation fires, whereas anthropogenic sources contribute less to the overall

55   transport of BC to Arctic regions (Bourgeois and Bey, 2011; Breider et al., 2014; Zhu et al., 2020). Nevertheless, anthropogenic BC sources in northern Eurasia can have important contributions to Arctic near surface concentrations, whereas South Asian BC layers are present in the Arctic middle and upper troposphere (Singh et al., 2010; Huang et al., 2010; Bourgeois and Bey, 2011; Sobhani et al., 2018). Regarding high-latitude anthropogenic sources, recent studies demonstrated gas flaring and shipping to significantly impact the lower tropospheric BC, organic, and sulfate aerosol burdens (e.g., AMAP, 2010; Chang et al.,

60   2011; Stohl et al., 2013; Eckhardt et al., 2013; Breider et al., 2014; Sand et al., 2016; Ferrero et al., 2016; Winiger et al., 2017; Xu et al., 2017; Gunsch et al., 2017; Leaitch et al., 2018; Creamean et al., 2018; Kirpes et al., 2018).

Although considerable advances had been achieved in recent years, our understanding of the aerosol vertical structure and related particle sources remains incomplete, partly owing to a paucity of detailed in-situ observations in summertime Arctic regions. In particular, airborne studies that attribute aerosol physical and chemical properties to sources are sparse, especially

65   in summer (Radke and Hobbs, 1989; Brock et al., 1989; Paris et al., 2009; Schmale et al., 2011; Quennehen et al., 2011; Kupiszewski et al., 2013; Creamean et al., 2018). Previous findings from ground-based and shipborne measurements might underestimate the relative role of aerosol long range transport from mid-latitude sources, due to the isolated nature of the summertime Arctic BL. Our study focuses on processes and sources controlling summer Arctic aerosol, using vertically resolved measurements of aerosol properties and trace gases, together with Lagrangian air mass history analysis. To our knowledge,

70   this is the first comprehensive source attribution study of summertime Arctic aerosol composition, combining airborne single particle and bulk chemical composition methods.

2   Experimental and Modeling Methods

2.1   Airborne Arctic field experiment NETCARE 2014

Motivated by limited knowledge of summertime Arctic aerosol processes, the aircraft campaign NETCARE 2014 took place

75   from Resolute Bay, Nunavut (Canada) from 4 - 21 July 2014. This was part of the NETCARE project (Network on Climate and Aerosols: Addressing Key Uncertainties in Remote Canadian Environments; Abbatt et al., 2019). Resolute Bay faces the Northwest Passage with Lancaster Sound near Baffin Bay and Nares Strait (see Fig. 1 in Köllner et al., 2017). Airborne measurements of aerosol physical and chemical properties, trace gases as well as meteorological parameters were performed onboard the AWI Polar 6 aircraft, a DC-3 aircraft modified to a Basler BT-67 for operation in cold and harsh environments

80   (Herber et al., 2008). Eleven flights were conducted from Resolute Bay (see Fig. S1). The total sampling time was about 44 hours of which roughly half of the time has been spent each in the BL and the FT. Flight tracks covered altitudes typically up to 3.5 km, while the flight on 8 July reached altitudes up to 6 km.

The measurements took place largely over remote areas characterized by open water (Lancaster Sound and polynyas north of Resolute Bay), sea ice, and Arctic vegetation (see Fig. 1 in Köllner et al., 2017). The sharp transition between open water and

85 sea ice was situated approximately 150 km south-east of Resolute Bay (see Fig. S1). Local anthropogenic pollution might have affected the measurements, but is primarily related to the sparse Arctic settlements with domestic activities, traffic, landfill and waste burning as well as local airports, and electric power generators (Aliabadi et al., 2015). The nearest neighboring communities are Arctic Bay and Grise Fjord approximately 360 km from Resolute Bay. In summary, the remoteness of the Resolute Bay region provided a well suited location for studying the pristine summertime Arctic atmosphere with access to

90 open water regions.

2.2 Aerosol particle composition measurements

2.2.1 Single particle mass spectrometer - ALABAMA

The Aircraft-based Laser ABlation Aerosol MAss spectrometer (ALABAMA) was deployed on the Polar 6 aircraft during the Arctic field experiment, to provide on-line measurements of single particle chemical composition and size. The instrument has

95 been described before in detail (Brands et al., 2011; Roth et al., 2016; Schmidt et al., 2017; Köllner et al., 2017) and is only briefly reviewed here. Particles enter the system through a critical orifice (for details see Molleker et al., 2020). The following Liu-type aerodynamic lens focuses particles into a narrow beam (Liu et al., 1995a, b, 2007). Further, particles are optically detected by scattering light when passing through two orthogonal detection laser beams ($\lambda = 405$ nm). The scattered light is focused by elliptical mirrors and further detected by photomultiplier tubes. This setup provides the particle's time of flight and

100 thus its velocity. The vacuum aerodynamic diameter (d_{va}) can be derived from the velocity, using a calibration with particles of known size, density, and shape (here, monodisperse PSL particles in a size range between 190 nm and 800 nm). During NETCARE 2014, the ALABAMA analyzed particles in a size range between 320 nm and 870 nm (d_{va}). The lower and upper size cut-offs are defined by the size range that include 98 % of all particles analyzed during NETCARE 2014. The successfully detected and sized particles are ablated and ionized in the high-vacuum region by a single triggered laser shot ($\lambda = 266$ nm). The

105 generated ions are guided into a Z-shaped Time-of-Flight mass spectrometer that provides bipolar mass spectra of individual particles. Details on the data analysis can be found in Sect. 2.4

2.2.2 Aerodyne High-Resolution Time-of-Flight aerosol mass spectrometer - HR-ToF-AMS

Sub-micron ensemble aerosol composition in a size range between 75 and 900 nm was measured by an Aerodyne High-Resolution Time-of-Flight aerosol mass spectrometer (HR-ToF-AMS), complementary to the ALABAMA single particle anal-

110 ysis. The HR-ToF-AMS is based on particle thermal vaporization by contact with a heated surface (~ 650 °C) followed by electron impact ionization (e.g., DeCarlo et al., 2006), in contrast to the ALABAMA laser-induced ablation/ionization process. The HR-ToF-AMS allows quantitative mass concentration measurements of non-refractory aerosol particle components. In practice, organic matter, nitrate, sulfate, ammonium, and methanesulfonic acid (MSA) are detected. To note, we further present the ratio of organic-to-sulfate mass concentrations measured by the HR-ToF-AMS. For further details see Willis et al. (2016,

115 2017) and Table S3. Both aerosol mass spectrometers, the ALABAMA and the HR-ToF-AMS, were not operated at altitudes
above 3.5 km to avoid damages under low pressure conditions in the cabin.

2.2.3 Single Particle Soot Photometer - SP2

Concentration of particles containing refractory black carbon (rBC) was acquired with a Single Particle Soot Photometer (SP2)
manufactured by DMT (Schwarz et al., 2006; Gao et al., 2007). The instrument includes a continuous intra-cavity Nd:YAG
120 laser ($\lambda = 1064$ nm) to classify individual particles as incandescent. The peak incandescence signal is linearly related to rBC
mass. For further details see Schulz et al. (2019) and Table S3.

2.3 Complementary experimental methods

Meteorological and state parameters were measured by the AIMMS-20 by Aventech Research Inc., integrated on the Polar 6
aircraft. The module Air-Data Probe provides temperature, pressure, relative humidity, wind direction, wind speed, and the
125 three-dimensional aircraft-relative flow vector (true air speed, angle of attack, and side slip). The second module, a GPS, pro-
cesses satellite navigation signals and determines aircraft three-dimensional position and altitude (Aventech, 2018).
Carbon monoxide (CO) mixing ratios were measured by an Aero-Laser ultra-fast CO monitor (model AL 5002), based on the
fluorescence of CO in the vacuum ultraviolet (VUV) at 150 nm (Scharffe et al., 2012; Aero-Laser GmbH, 2013; Wandel, 2015;
Bozem et al., 2019). Here, CO is used as an indicator of air mass influenced by combustion sources, including fossil fuel, and
130 biomass burning combustion (Andreae and Merlet, 2001). Further details can be found in Bozem et al. (2019) and Table S3.
Number concentrations of particles between 85 nm and 1000 nm were measured with the Ultra-High Sensitivity Aerosol Spec-
trometer (UHSAS), manufactured by DMT. The instrument is based on particle light scattering technique. Particles that cross
the beam of a laser ($\lambda = 1054$ nm) are counted and sized by their scattering signals. The intensity of the scattered light provides
information on the optical diameter (d_{opt}) (e.g., Cai et al., 2008; Schulz et al., 2019). For further details see Schulz et al. (2019)
135 and Table S3. Hereafter, only number concentration in a size range between 320 nm and 870 nm ($N_{>320}$) are used (see Sect.
2.4). Details on sampling strategy and inlet setups are discussed in detail by the following related publications: Leaitch et al.
(2016); Willis et al. (2016, 2017); Aliabadi et al. (2016b); Burkart et al. (2017); Köllner et al. (2017); Bozem et al. (2019);
Schulz et al. (2019).

2.4 Analysis of the ALABAMA single particle mass spectrometer data

140 The marker ion method is used to classify particles measured by the ALABAMA (see Köllner et al., 2017). The ion marker
method classifies particles based on the presence of pre-selected species that are of interest. This approach is not dependent on
the absolute value of the ion peak areas within one spectrum, but only on the presence of a certain ion peak area above a defined
threshold value. In principle, four analysis steps are required. First, a pre-selection of chemical compounds that are of interest
for the study is necessary. Second, ion markers of laboratory-generated particles with known composition are compared to ions
145 from ambient particles detected during the field experiment. Third, a threshold for the ion peak area is determined to distinguish

Table 1. Particle classification by marker species and associated ion markers applied in this study. References from laboratory and field studies using single particle mass spectrometry are indicated by numbers that are defined below. This table is partly adapted from Köllner et al. (2017).

Marker species (abbreviation)	Ion markers	References (lab/field)	Comments
Trimethylamine (TMA)	m/z +59 $((CH_3)_3N^+)$ and +58 $(C_3H_8N^+)$	1,2/3,4,5	
Sodium and/or chloride and/or nitrate (Na/Cl/Nitrate)	m/z +23 (Na^+) and (at least two of the following ions) +46 (Na_2^+), +62 (Na_2O^+), +63 (Na_2OH^+); (at least one of the following isotopic patterns/ions) +81/83 (Na_2Cl^+), -35/37 (Cl^-), -93/95 $(NaCl_2^-)$, -46 (NO_2^-), -62 (NO_3^-)	6,7,8/9,3	Isobaric interference with MSA at m/z -95
Elemental carbon (EC)	(at least six of the following ions) m/z +36, +48, ..., +144 (C_{3-12}^+) and/or (at least six of the following ions) m/z -36, -48, ..., -144 (C_{3-12}^-)	7,8/3,10	Except m/z -96 due to isobaric interference with SO_4^-
Low-molecular weight dicarboxylic acids (DCA)	(at least one of the following ions) m/z -89 $(C_2HO_4^-)$, m/z -103 $(C_3H_3O_4^-)$, m/z -117 $(C_4H_5O_4^-)$	11/12,13,14	representative: oxalic acid malonic acid succinic acid
Nitrate (NO_3)	(at least one of the following ions) m/z -46 (NO_2^-), -62 (NO_3^-)	10,11/3,7	

Table 1. Given reference numbers are defined as follows: [1]Angelino et al. (2001),[2]Köllner et al. (2017),[3]Roth et al. (2016),[4]Healy et al. (2015),[5]Rehbein et al. (2011),[6]Prather et al. (2013),[7]Schmidt et al. (2017),[8]Brands (2009),[9]Sierau et al. (2014),[10]Brands et al. (2011),[11]Silva and Prather (2000),[12]Lee et al. (2003),[13]Sullivan and Prather (2007),[14]Yang et al. (2009).

the ion signal from background noise (for details see Köllner et al., 2017). Finally, internal and external mixtures of chemical compounds are distinguished by checking the respective ions occur in the same particle mass spectrum or in separate particle mass spectra. Both types of mixtures can be presented in a decision tree. The decision tree is structured as follows: upper/lower branches refer to positive/negative response for whether ion markers of the respective substance are above/below the ion peak threshold. This study focuses on five particle types based on the presence of the following substances (see Table 1): sodium

150
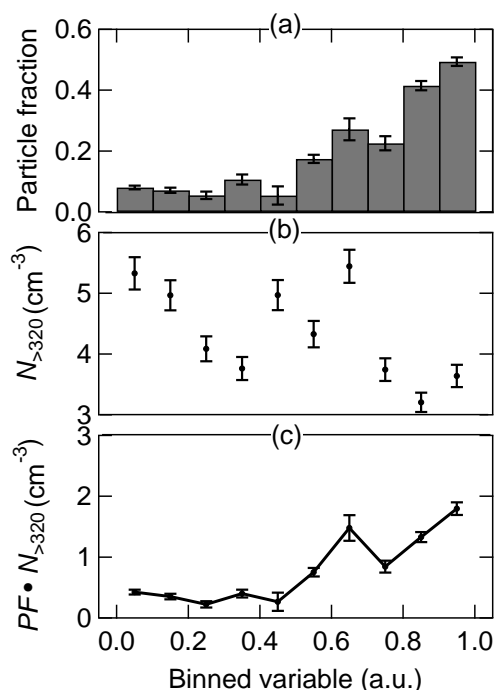
Figure 1. Example for the three-step scaling procedure. (a) The ALABAMA number fraction of the specific particle type (PF), (b) the averaged UHSAS number concentration in a size range between 320 nm and 870 nm ($N_{>320}$), (c) and the scaled ALABAMA number concentration ($PF \cdot N_{>320}$) are compared with variables that are simultaneously measured. In this study, we used the following variables: FLEXPART PES fractions, altitude, H/C ratio, O/C ratio, and CO mixing ratio.

and/or chloride and/or nitrate (Na/Cl/Nitrate), elemental carbon (EC), nitrate (NO_3), trimethylamine (TMA), and dicarboxylic acids (DCA). We choose these substances because they are well suited to study aerosol sources as well as aerosol processing along transport that are the subject of this work, such as marine, vegetation fires, flaring, and other anthropogenic sources. We further analyzed ion peaks that might correspond to levoglucosan, but the marker ions are ambiguous (see Supplement Sect. 4). As a result, we will not discuss levoglucosan in this analysis.

The conversion of unscaled ALABAMA measurements into quantitative particle number concentrations allows for assigning particle types to different sources (Sullivan and Prather, 2005). Several studies using single particle mass spectrometry applied a similar scaling procedure (e.g., Qin et al., 2006; Healy et al., 2013; Gunsch et al., 2018; Froyd et al., 2019). Based on particle classification, the fraction of the ALABAMA particle types is calculated (Fig. 1a). To determine particle fractions, total analyzed (i.e., detected+ablated/ionized) particles and specific particle types that are of interest are categorized into bins of a simultaneously measured variable (see horizontal axis in Fig. 1). For each bin, the particle fraction is defined as the number of particles of the specific type divided by the number of all analyzed particles (PF; see Fig. 1a). Bin widths are chosen to guarantee an acceptable level of both statistical significance and resolution. Bins containing less than 20 spectra in total

were excluded from the analysis. Further, the particle fraction is scaled to number concentrations, using measurements of a
co-located quantitative reference instrument, here the UHSAS onboard the Polar 6 (see Sect. 2.3). The UHSAS number con-
centration in a size range between 320 nm and 870 nm ($N_{>320}$; Fig. 1b) is used. The selected UHSAS lower and upper size
cut offs refer to the ALABAMA size range measured during NETCARE 2014 (see Sect. 2.2). Conceptually, scaled number
concentrations of the ALABAMA particle types are determined by multiplying the particle fraction with the averaged UHSAS
number concentration in each bin ($PF \cdot N_{>320}$; Fig. 1c).

By using this scaling method, it is assumed that the d_{opt} measured by the UHSAS and the d_{va} measured by the ALABAMA are
equal. It is further assumed that the ALABAMA transmits, detects, and ablates/ionizes all particles with the same efficiency.
These assumptions introduce uncertainties in the scaled number concentrations, as the detection efficiency (DE) and the hit
rate are observed to be dependent on several factors. The DE is size-dependent, mainly caused by the transmission efficiency
of the aerodynamic lens and the optical detection (Zhang et al., 2004; Liu et al., 2007; Brands et al., 2011). However, a size-
dependent scaling factor was not deployed in this study, owing to the low particle counting statistics per bin. As a result, the
scaling method may lead to uncertainties when determining the concentration of particles smaller than approximately 400 nm.
Likewise, the hit rate in laser ablation/ionization technique is dependent on various particle characteristics, such as size, com-
position, and shape (Thomson et al., 1997; Kane et al., 2001; Moffet and Prather, 2009; Brands et al., 2011). The hit rate can
thus vary during ambient measurements, which may cause a problem when interpreting the fraction of particle types. Further
details on the hit rate variability during NETCARE 2014 are given in the Supplement Sect. 1.

Given that the scaled number concentration is estimated under several assumptions, we solely discuss trends in number concen-
trations in comparison with other parameters to identify sources of different particle types, rather than discussing the absolute
number concentration. In addition, we will only discuss trends that are clearly visible in both the number fraction and scaled
concentration. For clarity, we focus on the scaled number concentration ($PF \cdot N_{>320}$) in the following sections. Additional
figures showing particle fraction and averaged UHSAS number concentration are in given in the Supplement Sect. 6.

2.5 Air mass history modeling

2.5.1 FLEXPART

Air mass history analysis is crucial for understanding aerosol sources and transport processes, both of which control aerosol
properties in Arctic regions. In this study, we use the Lagrangian FLEXible PARTicle dispersion model (FLEXPART, version
10.0). FLEXPART is a comprehensive tool for modeling atmospheric transport (e.g., Stohl, 1998; Stohl et al., 2003, 2005) and
is widely used in Arctic studies (e.g., Stohl, 2006; Paris et al., 2009; Schmale et al., 2011; Evangeliou et al., 2019; Zhu et al.,
2020). In this study, FLEXPART was operated backward in time with operational data from the ECMWF with 0.25° horizontal
and 3 hours temporal resolution as well as with 137 vertical hybrid sigma-pressure levels. Tracer air parcels (usually called
tracer particles) are released from a certain receptor location and followed for 15 days backward in time (Stohl et al., 2003;
Seibert and Frank, 2004; Stohl et al., 2005). The receptor location depends on airborne sampling location. In detail, releases
were initialized each 10-min sampling interval along the flight track. By this approach, between 16 and 29 releases were created

for each flight, depending on flight duration. The release volume of the tracer particles for each 10 min interval was set by the maximum and minimum geographic locations during this time segment. The main variable calculated by FLEXPART is the so-called Potential Emission Sensitivity (PES) that describes the sensitivity of air sampled at the receptor to source emission

200 locations (Seibert and Frank, 2004; Stohl et al., 2005; Hirdman et al., 2010). The PES value has the dimension of seconds and essentially is proportional to the parcel's residence time in a particular output grid cell (Seibert and Frank, 2004; Hirdman et al., 2010). It is assumed that each source contributes with unit strength in the respective cell. Further, the transported tracer is inert, which means no impact of precipitation and no chemical reactions are considered in FLEXPART (Stohl et al., 2003; Hirdman et al., 2010). The PES function is provided every six hours (i.e., 60 values for a 15 day backtrajectory), with uniform

205 horizontal grid spacing of 0.25°, and with five vertical levels (400, 1000, 2000, 5000, and 15000 m).

FLEXPART output combined with geographical locations of emission sources may provide a more detailed analysis of the relationship between Arctic aerosol composition and sources. This analysis requires the following data processing steps: First, the total residence time of air masses in each grid cell is obtained by integrating PES data in time for a given vertical layer. It is assumed that surface emissions into this vertical layer, the so-called footprint layer, are mixed instantaneously by turbulence

210 in the BL. Therefore, the lowest vertical level (0 - 400 m) is applied for most ground sources (e.g., Stohl et al., 2013), except for vegetation fires related to buoyant effects (see details in the Supplement Sect. 2.1). Second, we show maps that specify geolocations of source sectors and source regions (see Sect. 2.5.2). Third, the prior obtained two-dimensional (latitude and longitude) PES map is folded with the two-dimensional map of source regions and sectors. Finally, each grid cell is summed to obtain the total residence time of sampled air mass spent over a specific source within the 15 days prior to sampling and within

215 the vertical footprint layer. In general for this study, the PES fraction is defined as the ratio of the PES of sampled air above source regions/sectors within the footprint layer of the model domain over a 15-days integrated backward simulation compared to the PES of sampled air in the total vertical column of the model domain over a 15-days integrated backward simulation.

2.5.2 Source regions and sectors

Geolocations of selected source regions (e.g., Europe) and sectors (e.g., vegetation fires) are visualized by using two-dimensional

220 maps with horizontal grid spacing of 0.25°. Geographical regions that likely contribute to Arctic aerosol in summer comprise primarily northern Eurasia, North America, East Asia, and the Arctic itself. Based on several Arctic studies (Stohl, 2006; Shindell et al., 2008; Bourgeois and Bey, 2011; Liu et al., 2015; Yang et al., 2018), selected source regions are shown in Fig. 2. We consider Europe and Siberia as well as Alaska, northern Canada (nCa), and southern North America (sNA) separately due to differences in vegetation fire occurrence, industrial sources, flaring spots, and population density (Figs. 3a-d, respectively).

225 Large marine areas of the Pacific and Atlantic Oceans are included due to their vicinity to Arctic regions. Arctic regions are specified as located north of 73.5° N, based on the determination of the July 2014 polar dome location by Bozem et al. (2019). Details on creating maps (Fig. 3) that specify the geolocation of the following source sectors: vegetation fires, industry, flaring, population, and Arctic open water, are given in the Supplement Sect. 2. Briefly, for identifying vegetation fire spots, we used data from the Visible Infrared Imaging Radiometer Suite (VIIRS) onboard the Suomi National Polar-Orbiting Partnership

230 spacecraft. These measurements provide sub-pixel thermal anomalies by signals in mid- and thermal infrared spectral range
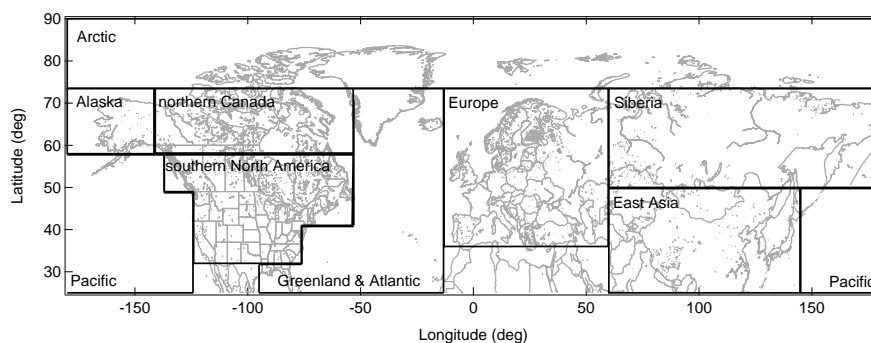
Figure 2. Map showing selected source regions: Arctic, Alaska, northern Canada, southern North America, Pacific, Greenland & Atlantic, Europe, Siberia, and East Asia.

(Schroeder et al., 2014; Schroeder and Giglio, 2018). However, thermal anomalies typically include both active vegetation fires and industrial heat sources by fossil-fuel combustion etc. Therefore, anthropogenic heat sources, such as industry, flaring, and densely populated regions, are separately mapped (as explained in the following) and subsequently excluded from the thermal anomaly map. Residual heat sources in Fig. 3a thus present vegetation fires. Industrial areas, including flaring, are obtained by using quantitative estimates of infrared source emission temperatures from the Nightfire product from VIIRS (Figs. 3b and c). This method is taking advantage of absent solar reflectance in short-wave infrared spectral range during night (Elvidge et al., 2013, 2016). Emission temperatures typically exhibit bimodal distributions by a combination of gas flares dominating the upper mode (peaking in the 1600 - 2000 K range) and other industrial heat sources as well as vegetation fires dominating the lower mode (peaking in the 800 - 1200 K range; Elvidge et al., 2016; Liu et al., 2018). Geo-located data on population are provided online (MaxMind, 2018). The criteria for the map grid cell to be classified as populated is given by more than 1000 people living in a 0.25° x 0.25° area (Fig. 3d). Finally, we used measurements from the Special Sensor Microwave Imager/Sounder (SSMIS) onboard the Defense Meteorological Satellite Program (DMSP) to assess sea ice coverage in July 2014 and by this Arctic open water areas (Fig. 3e). Data on sea ice coverage are based on detected brightness temperature (Cavalieri et al., 1996, updated yearly). In general, these approaches classify whether the source sector is present or absent in the grid cell irrespective from source strengths, rather than providing quantitative source-specified emission data.

3 Results and discussions

3.1 Meteorological overview and air mass history

Meteorological conditions combined with air mass history play a major role when understanding Arctic aerosol composition influenced by local as well as distant sources and transport. The synoptic situations during NETCARE 2014 have been discussed in previous publications (see Bozem et al., 2019; Burkart et al., 2017; Köllner et al., 2017; Leaitch et al., 2016). Air mass history derived by FLEXPART is summarized in Figs. 4 and 5 as a function of sampling altitude. The synoptic conditions
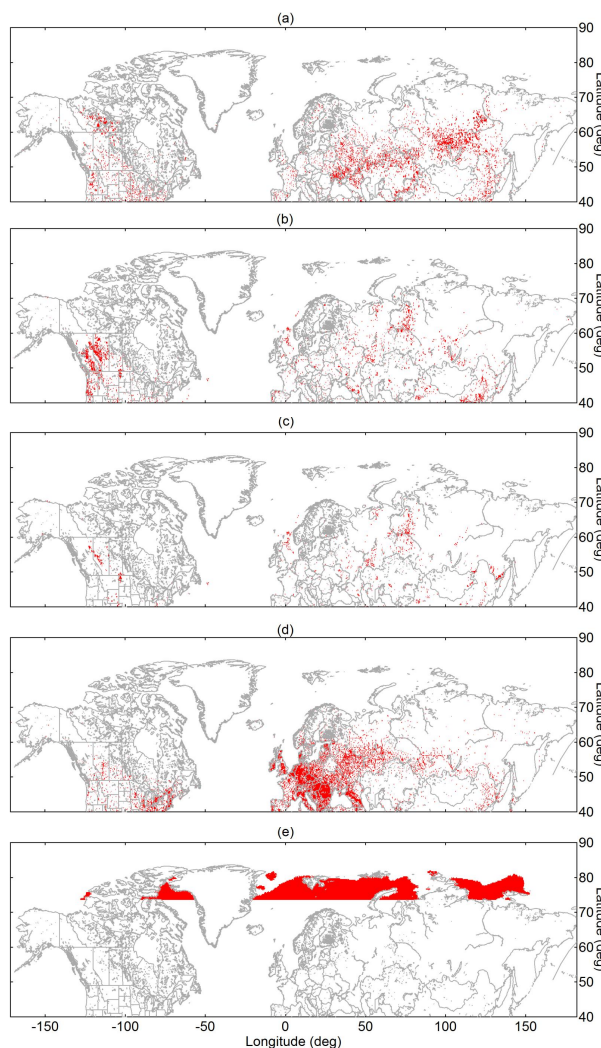
Figure 3. Map showing the geolocation of selected source sectors: (a) vegetation fires, (b) industry (including flaring), (c) flaring, (d) population, and (e) Arctic open water. Panel (a) shows accumulated fires for 19 June until 21 July 2014. Red pixels indicate the presence of the respective source sector irrespective of the particular emission strength.

changed over the course of NETCARE 2014 from an initial Arctic air mass period (July 4-12) to a southern air mass period (July 17-21) with a transition in between (Burkart et al., 2017; Bozem et al., 2019). Since this has a significant impact on the distributions of the observed quantities, we analyze the measurements for each period individually.

255 ### 3.1.1 Arctic air mass period

During the Arctic air mass period, the measurement region was under the influence of a prevailing high-pressure system generally clear skies, some low-level stratocumulus clouds (Leaitch et al., 2016), low wind speeds, and a stable stratified
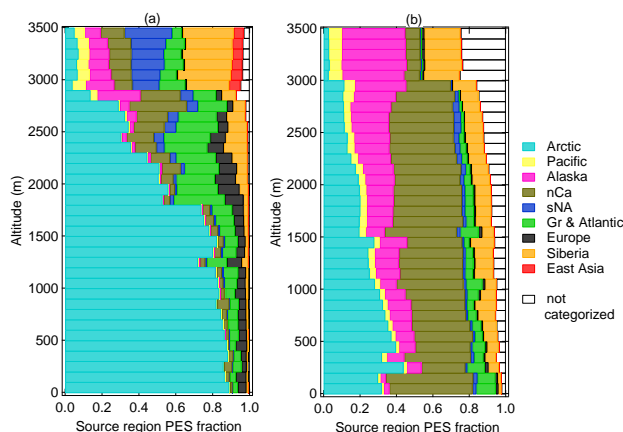
Figure 4. Vertically resolved cumulative contribution of source regions to sampling altitude during (a) the Arctic and (b) the southern air mass periods. The FLEXPART derived contribution is expressed as a fraction of the potential emission sensitivity (PES) in the model domain lowest vertical level (0 - 400 m) over a 15-days backward simulation. Acronyms are defined as follows: nCa = northern Canada; sNA = southern North America; Gr = Greenland. The white parts depict areas that are not categorized in the selected geographical regions.
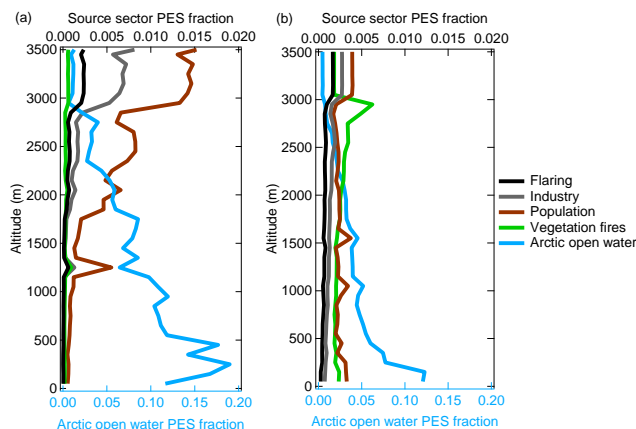
Figure 5. Vertically resolved cumulative contribution of source sectors to sampling altitude during (a) the Arctic and (b) the southern air mass periods. The FLEXPART derived contribution is expressed as a fraction of the potential emission sensitivity (PES) in the model domain lowest vertical level (0 - 400 m) over a 15-days backward simulation. The PES above vegetation fires refers to the 1 - 5 km vertical range. Bottom and top axes represent PES fractions of Arctic open water and other source sectors, respectively.

shallow BL (Bozem et al., 2019). Inferred from the vertical profile of pseudoequivalent potential temperature, the local upper BL height was on average between 250 m and 450 m, including a surface-based temperature inversion (Köllner et al., 2017). Air mass history during the first period reflects the concept of isentropic transport to Arctic regions. Near-surface regions are largely isolated from the rest of the atmosphere and regions aloft are episodically influenced by air originating from southern latitudes (Fig. 4a). The distinct change in air mass history at around 3 km altitude depicts the transition to measurement regions

located outside of the polar dome (Fig. 4a; Bozem et al., 2019).

The period is referred to as Arctic air mass period since air mass history 15 days prior to sampling shows a dominant influence

265 of air masses from the high Arctic. Inside the BL, we predominantly sampled air masses that had resided in the Arctic regions (up to 90 % in Fig. 4a). Particularly, a significant fraction of the high Arctic air masses has resided over open water (up to 20 % in Fig. 5a). Thus, air masses inside the BL originated to a large degree from pristine Arctic regions with mainly natural aerosol sources affecting composition. Above the BL, influences of Arctic air masses were still pronounced (Fig. 4a). However, contributions from southern latitude regions, i.e. Europe, Siberia, northern Canada, Greenland, and the Atlantic

270 Ocean, increased with altitude due to enhanced quasi-isentropic transport from these regions into the high Arctic (Fig. 4a; e.g., Klonecki et al., 2003). An example of such a transport from Europe towards the Arctic is shown in Figure S35. Air masses at low levels over Europe ascended along the upward sloping isentropes when they were transported polewards. Thus, the impact of the emissions from these source regions on our measurements becomes apparent at higher altitudes (Fig. 5a). Air mass history above 3 km altitude, above the polar dome (Bozem et al., 2019), indicates a sharp transition to a dominating influence

275 of mid-latitude air masses (Fig. 4a). Consistent with several modeling studies, contributions of regions south of 50-60° N (i.e., East Asia, Pacific, and southern North America) became significantly important only above 3 km, whereas sources in Europe and northern Canada frequently affected measurements in lower altitudes (e.g., Bourgeois and Bey, 2011; Sobhani et al., 2018; Yang et al., 2018). Thus, anthropogenic pollution in altitudes above 3 km can be attributed to sources in East Asia and southern North America (compare Figs. 4a and 5a). In general during the Arctic air mass period, the contribution of vegetation fires was

280 negligible (Fig. 5a). This finding is in line with low CO mixing ratios ($< 90\,\text{ppb}_\text{v}$) measured during the first period (Bozem et al., 2019).

3.1.2 Southern air mass period

Meteorological conditions changed after 12 July due to a low-pressure system that was initially centered to the west above the Beaufort Sea and finally passed through Resolute Bay on 15 July. Until 17 July, flying was impeded by the local weather

285 situation with low visibility, fog, and precipitation along with the low-pressure system (Burkart et al., 2017). However, the measurement region was increasingly impacted by an intense low-pressure system located south of Resolute Bay that led to a different meteorological situation during the period from 17 - 21 July (Bozem et al., 2019). Meteorological conditions were characterized by overcast sky, occasional precipitation, moist air throughout the lower troposphere, higher wind speeds, and warmer temperatures compared to the Arctic air mass period (Burkart et al., 2017; Bozem et al., 2019). The BL was more

290 difficult to identify compared to the prior period due to a less well defined temperature inversion. According to the detailed BL study by Aliabadi et al. (2016a), the BL height reached altitudes between approximately 200 m and 400 m. However, vertical mixing between the BL and FT was likely promoted caused by a combination of less intense temperature inversions, higher wind speeds, warmer temperatures, and a higher abundance of clouds compared to the first period (e.g., Stull, 1997; Fuelberg et al., 2010; Tjernström et al., 2012).

295 This period is referred to as southern air mass period, since air mass history shows the prevalence of air masses originating from southern latitudes. Lagrangian air mass history analysis suggests a pronounced impact of southern latitude sources on

Figure 6. Classification of 10137 single particle spectra based on the ion marker method and illustrated with the decision tree (see Sect. 2.4). Upper/lower branches refer to the presence/absence of substances in the particle mass spectra. Numbers are given as relative abundances in % normalized to 10137 particles. The initial classification provides three groups of particle mass spectra with dual-, single positive, and single negative polarity. Particle types, indicated by colors, contain: Na/Cl/Nitrate (dark blue), EC (black), non-sea-spray-(nss)-NO_3 (light blue), trimethylamine (TMA) (yellow), dicarboxylic acids (DCA) (brown), and "Others" (gray). As an example, 4 % of 10137 particles (indicated by the asterisk) contain DCA and nss-nitrate (from right to left).

Arctic composition (Figs. 4b and 5b). First, the cumulative contribution of all regions outside the Arctic dominated air mass history within the lower troposphere, making up to 97 % of the PES (Fig. 4b). Along with this, northern Canada and Alaska exerted the largest influences and the European influence was smaller than during the first period, consistent with the prevailing

300 cyclonic activity south of Resolute Bay. Transport of air masses from northern Canada was accompanied by emissions from vegetation fires in the Great Slave Lake region (compare Figs. 3a and S36). Contributions from industrial and flaring activities were likely accompanied by transport of air masses from Alaska, Siberia, southern North America, and Europe (Figs. 4b and 5b). Also, the contribution of air masses that had resided above Arctic open water was significantly lower during the southern air mass period (Fig. 5b), compared to the Arctic air mass period. The representativeness of both July 2014 measurement

305 periods with respect to climatological conditions is discussed in the Supplement Sect. 3. Briefly, synoptic situations during the Arctic air mass period were generally consistent with the climatology, whereas the southern air mass period with influences of the low-pressure system were significantly anomalous compared to climatological mean.

Figure 7. Bipolar mean spectra of the ALABAMA particle types: (a) Na/Cl/Nitrate-containing (195 particles out of 10137 ≙ 2 %), (b) EC-containing (188 particles out of 10137 ≙ 2 %), (c) nss-nitrate-containing (688 particles out of 10137 ≙ 7 %), (d) TMA-containing (2325 particles out of 10137 ≙ 23 %) and (e) DCA-containing (3150 particles out of 10137 ≙ 31 %).

3.2 Single particle chemical composition

By means of the ALABAMA, 10137 particles were analyzed during the NETCARE 2014 study when sampling outside clouds;
310   94 % of the spectra include size information; 78 % of the spectra have dual polarity (Fig. 6). Potential reasons for the lack of negative ions are discussed in Köllner et al. (2017). It might be that single-polarity spectra are preferably produced in high relative humidity environments (Neubauer et al., 1998; Spencer et al., 2008), in particular in marine environments (Guasco et al., 2014). Particle classification by the ion marker method introduced in Sect. 2.4 is illustrated here by means of a decision tree in Fig. 6. Particle groups that include less than 300 particles (~ 3 %) are not further sub-classified due to the low counting
315   statistics. This means EC- and Na/Cl/Nitrate-containing particles are excluded from other types due to their low number. In contrast, particles that contain substances such as nitrate, TMA, and/or DCA and that are externally mixed from EC and Na/Cl can be assigned to several types. TMA- and DCA-containing particles are the most prominent types with relative contributions of 23 % and 31 % to the total number of analyzed particles, respectively (indicated by yellow and brown filling in Fig. 6). In contrast, particles containing Na/Cl/Nitrate, EC, and nitrate (externally mixed from Na and Cl) account for 2 %, 2 %, and 7 %,
320   respectively. In this analysis, 46 % of all mass spectra are not included in the particle classification (gray filling in Fig. 6). The mean spectrum of those "Others" primarily shows peaks of potassium and sulfate (Fig. S9). In the following, mean spectra of the main particle types (Fig. 7) combined with additional ion signals (Table S2) provide an overview of the averaged chemical composition.

The term particulate DCA implies the presence of oxalic, malonic, and/or succininc acid (see Table 1), with oxalic acid as most
325   abundant (86 %), followed by succinic acid with 41 % and malonic acid with 38 % (not shown). In addition, the majority of the DCA spectra show the concurrent presence of oxidized organics at m/z -45, -59, -71, and -73 (Fig. 7e and Table S2). From our ALABAMA analysis, we can infer that particulate DCA was partly internally mixed with particles containing sodium, chloride, and/or nitrate (Na/Cl/Nitrate), which are interpreted as sea spray particles (Table S2 and Fig. S8). In detail, the presence of DCA was found in 60 % of those sea spray particles. The presence of DCA together with sea spray had been observed earlier
330   during measurement campaigns with focus on marine air (Sullivan and Prather, 2007), also in Arctic regions (Kerminen et al., 1999). However, the majority of DCA were externally mixed from sea spray (Figs. 6 and 7e). Moreover, 14 % of those DCA-containing particles (without sea spray) were internally mixed with TMA and MSA (Figs. 6 and 7e). In our prior study, we concluded that particulate TMA in the Arctic summer results from secondary formation, owing to the external mixture of TMA and primary components, such as sodium (Köllner et al., 2017). Thus, together with the secondary nature of TMA and MSA
335   (Hoffmann et al., 2016), the internal mixture of DCA with TMA and MSA suggests that DCA results from the secondary (potentially aqueous) conversion of precursor gases (e.g., Kawamura and Bikkina, 2016).

Nitrate was also externally mixed with sea spray particles, hereafter referred to as non-sea-spray (nss)-nitrate. The averaged chemical composition of EC- and nss-nitrate-containing types provide evidence for internal mixing with secondary substances such as sulfate, MSA, and oxygen-containing organic matter (OM; Figs. 7b-c and Table S2). In addition, 20 % of the EC
340   particles were internally mixed with nitrate (Fig. 7b and Table S2). More than 50 % of the nss-nitrate- and EC-containing particle spectra include ion signals of DCA (Fig. 6), particularly oxalic acid at m/z -89 (Fig. 7b-c).
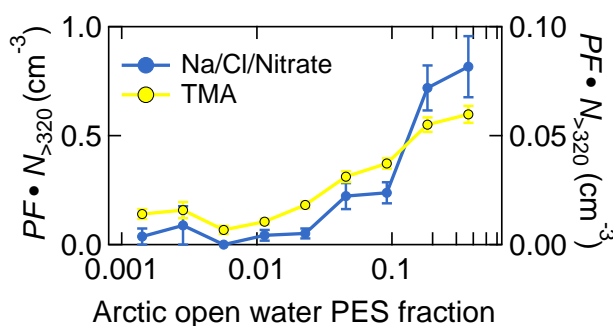
Figure 8. Aerosol composition measured by the ALABAMA as a function of FLEXPART derived residence time over Arctic open water areas during the Arctic air mass period. The panel represents the ALABAMA scaled number concentration ($PF \cdot N_{>320}$) with right axis referring to Na/Cl/Nitrate-containing (blue) and left axis referring to TMA-containing (yellow) particles. Uncertainty analyses are given in the Supplement Sect. 7.

3.3 Arctic marine influences on particle composition

The clean and pristine Arctic background conditions during the first period (Fig. 4) provide the unique opportunity to study the influence of Arctic marine sources on particle composition. This section complements the results presented in Köllner et al. (2017) and Willis et al. (2017), both analyzing particle chemical composition during the first period. It was shown that marine processes dominated the presence of organic matter and MSA in low sulfate environments in the summertime Arctic BL (Willis et al., 2017; Köllner et al., 2017). The organic-to-sulfate and MSA-to-sulfate ratios peaked when the residence time over Arctic open water region was highest (Willis et al., 2017). As a new analysis compared to our prior studies, we present the aerosol composition measured by the ALABAMA as a function of FLEXPART derived residence time over Arctic open water areas in Fig. 8 and the vertically resolved aerosol composition in Fig. 9. Particulate TMA was predominantly abundant when the air resided for more than 8 days prior to sampling over Arctic open water areas (Fig. 8). Along with the marine influence, Na/Cl/Nitrate-containing particles were largely abundant when the residence time over Arctic open water regions was high (Fig. 8), linking those particles to locally emitted sea spray. In addition, both particle types are predominantly present in the Arctic marine BL (Fig. 9). Taken together, air mass history demonstrates that Arctic marine sources contributed to the abundance of particulate TMA internally mixed with MSA, sulfate, and/or other organics as well as sea spray particles in the summertime marine Arctic BL.

3.4 Long range transport influences on particle composition

In a next step, we will focus on the particle composition measured in the summertime Arctic lower FT. In contrast to particle composition in the Arctic marine BL, our analysis suggests that particle composition in the Arctic FT was much more influenced by long range transport (see Sect. 3.1). To illustrate this, we show the vertically resolved aerosol composition in Fig. 10 and the aerosol composition as a function of FLEXPART derived air mass residence time over different geographical regions
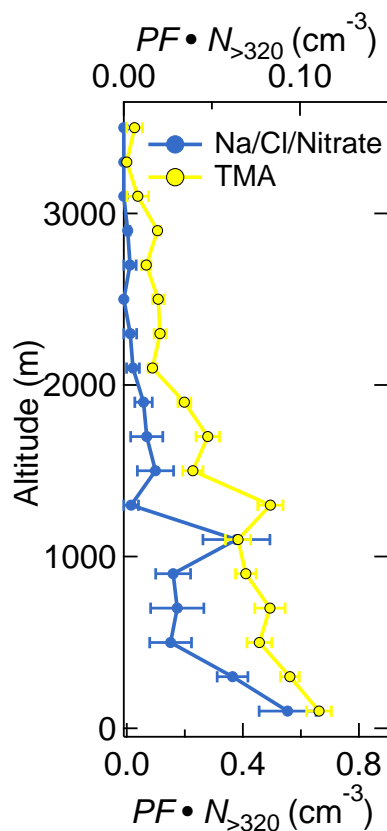
Figure 9. Vertically resolved aerosol composition measured by the ALABAMA during the Arctic air mass period. The panel represents the ALABAMA scaled number concentration ($PF \cdot N_{>320}$) with top axis referring to Na/Cl/Nitrate-containing (blue) and bottom axis referring to TMA-containing (yellow) particles. Uncertainty analyses are given in the Supplement Sect. 7.

in Fig. 11.

Particularly during the Arctic air mass period, the ALABAMA analysis suggests that organic matter in the FT was partly composed of particulate DCA. The number concentration of DCA-containing particles was increasing with increasing altitude

365 (Fig. 10a). Further, Figs. 12 and 13 show the number concentrations of DCA-containing particles in comparison with the HR-ToF-AMS estimated oxygen-to-carbon (O/C) and hydrogen-to-carbon (H/C) ratios as well as with the FLEXPART derived air mass residence time over Arctic regions, respectively. The abundance of DCA-containing particles coincided with air masses with more oxidized organic matter (Fig. 12). Consistent with this result, the size of DCA particles was larger compared to other particle types (Fig. S11). Finally, air mass history shows that the abundance of DCA-containing particles correlated with

370 time spent outside Arctic regions (Fig. 13). This result is in line with findings of an Arctic airborne study by Schmale et al. (2011), indicating low-volatility highly oxygenated aerosol in pollution plumes from lower latitudes. However, no significant trend with a distinct source region outside the Arctic was found (not shown), as expected from the variety of biogenic and
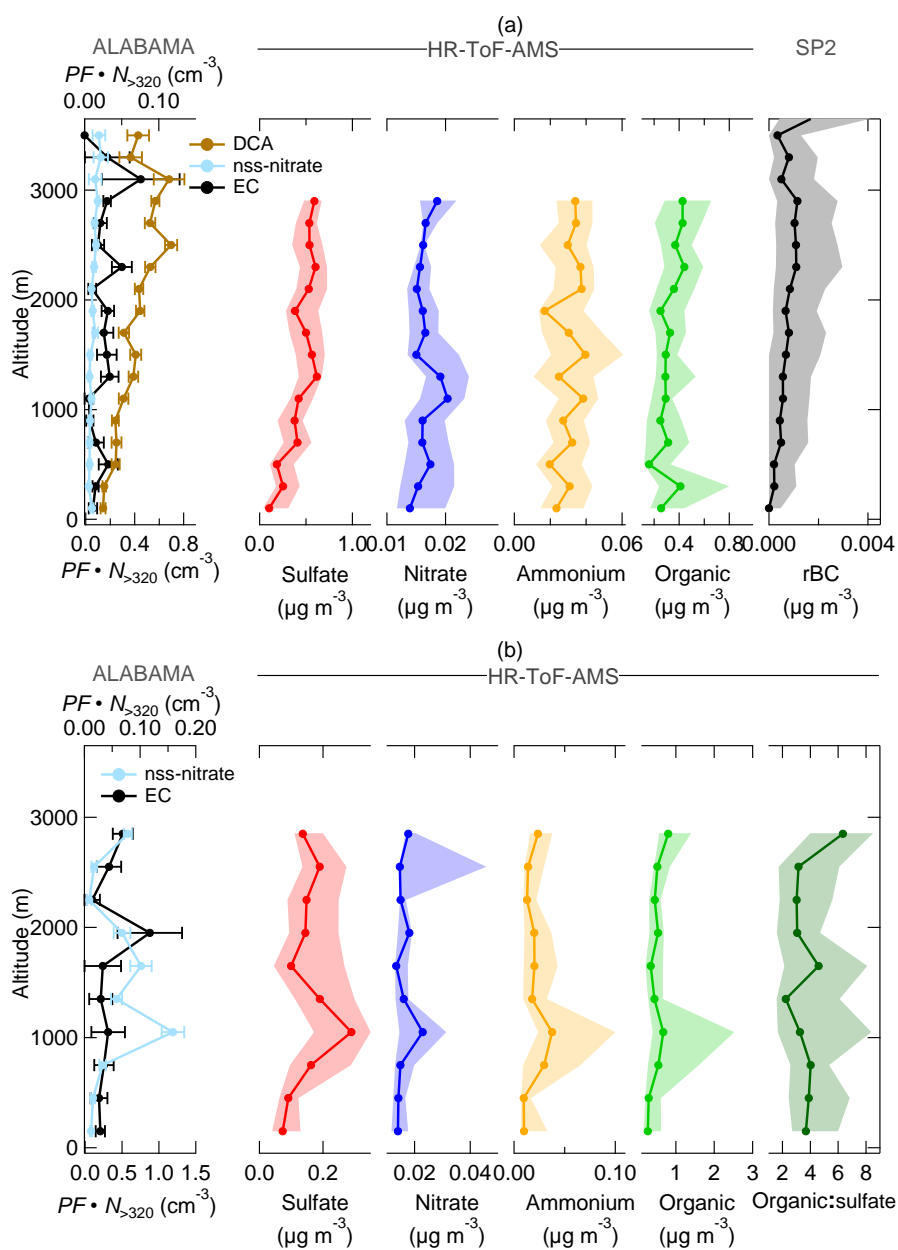
Figure 10. Vertically resolved aerosol composition measured by the ALABAMA, by the HR-ToF-AMS, and by the SP2 (indicated on the top side) during (a) the Arctic and (b) the southern air mass periods. Note the different scales. Left panel represents the ALABAMA scaled number concentration ($PF \cdot N_{>320}$) with top axis referring to EC-containing (black) and bottom axis referring to nss-nitrate (light blue) - and DCA (brown) -containing particles. Right panels represent each median (solid line with marker) and interquartile ranges (shaded area) of the HR-ToF-AMS mass concentrations of sulfate (red), nitrate (blue), ammonium (orange), organic matter (light green), and the organic-to-sulfate ratio (dark green) as well as the SP2 mass concentration of refractory black carbon (rBC) (black). Uncertainty analyses are given in the Supplement Sect. 7.
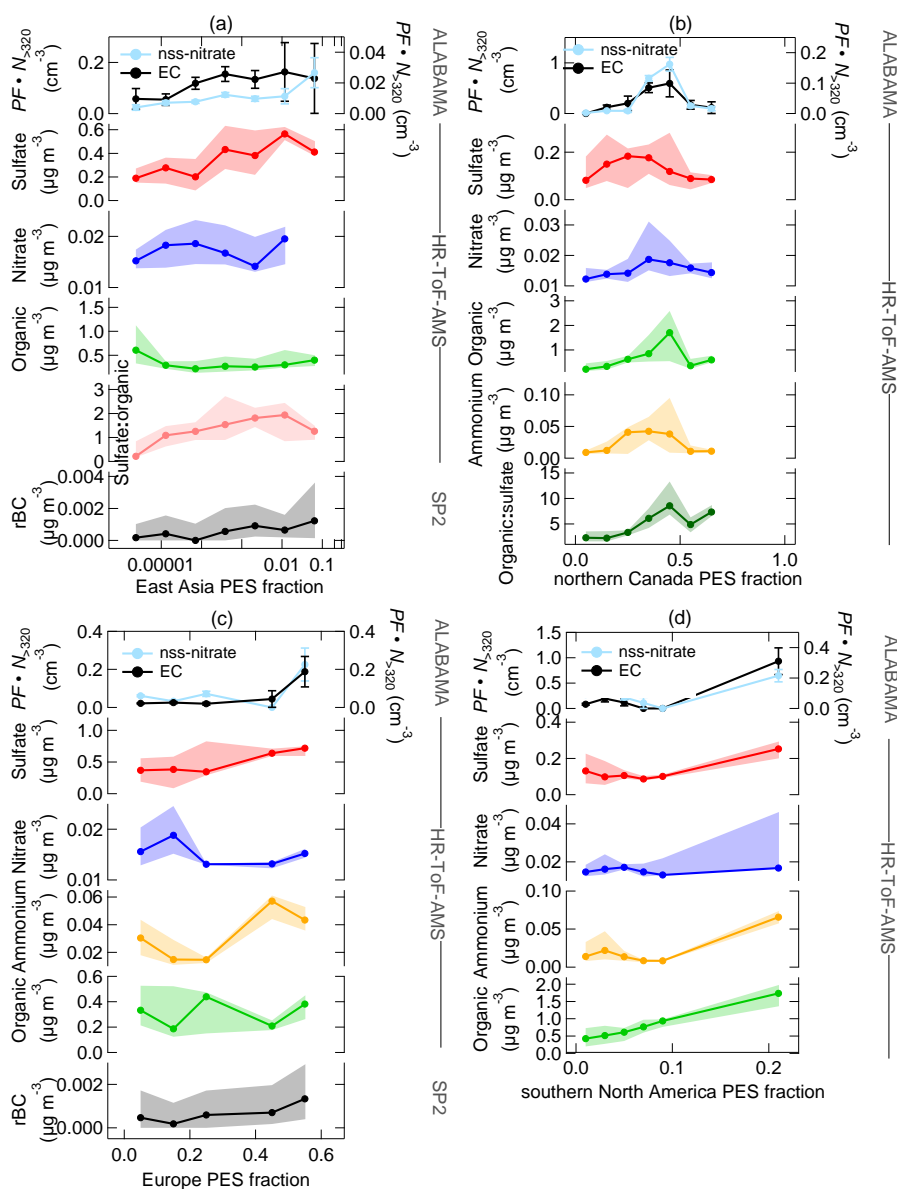
Figure 11. Aerosol composition measured by the ALABAMA, by the HR-ToF-AMS, and by the SP2 (indicated on the right side) as a function of FLEXPART derived air mass residence time over the East Asia (a), northern Canada (b), Europe (c), and southern North America (d) during the Arctic (a,c) and the southern air mass (b,d) periods. Top panel represents each the ALABAMA scaled number concentration ($PF \cdot N_{>320}$) with right axis referring to EC-containing (black) and left axis referring to nss-nitrate-containing (light blue) particles. Lower panels represent each median (solid line with marker) and interquartile ranges (shaded area) of the HR-ToF-AMS mass concentrations of sulfate (red), nitrate (blue), ammonium (orange), organic matter (light green), the sulfate-to-organic ratio (pink), and the organic-to-sulfate ratio (dark green) as well as the SP2 mass concentration of refractory black carbon (rBC) (black). Uncertainty analyses are given in the Supplement Sect. 7.

anthropogenic precursor gases as well as primary emissions. However, direct observations of DCA in Arctic regions were up to now confined to measurements in the BL (e.g., Shaw et al., 2010; Kawamura et al., 2012; Leaitch et al., 2018), suggesting

375 summer minimum concentrations due to a combination of diminished transport of precursors and more efficient aerosol wet removal compared to other seasons. Along with results in our study and the stable stratified nature of the Arctic BL, it is likely that that these previous BL studies were not sensitive to the presence of organic acids in the Arctic FT influenced by long range transport. Besides the presence of particulate DCA in the FT, DCA-containing particles internally mixed with TMA and MSA (see Sect. 3.2) were largely present in the stable stratified BL (Fig. S12) and when the residence time within the Arctic

380 was high (Fig. S13), indicating sources of particulate DCA in the summertime Arctic. This finding is consistent with previous ground-based and shipborne studies, linking the abundance of DCA in the summertime Arctic to regional Arctic sources (e.g., Kawamura et al., 1996; Kerminen et al., 1999; Kawamura et al., 2010, 2012).

Aerosol transport from lower latitudes further influenced Arctic composition by particles that contained nitrate and EC. Both species were more pronounced in the FT compared to the BL (Fig. 10). Comparing both periods, the nitrate and organic con-

385 centrations measured by the ALABAMA and HR-ToF-AMS were higher during the southern air mass period (compare Figs. 10a and b), reflecting the pronounced influence of vegetation fires during this time (see Sect. 3.1.2). Consistently, particles containing nitrate were predominantly present when the residence time over northern Canada was high (Fig. 11b). However, also during the Arctic air mass period, the abundance of nss-nitrate measured by the ALABAMA can be assigned to aerosol transport from lower latitudes (Figs. 11a and c). Air mass history shows contributions from East Asia and Europe to aerosol

390 composition during the Arctic air mass period (Figs. 11a and c, respectively). Figure S33 presents an example of the FLEX-PART derived transport pathway from East Asia (particularly Japan) to the Arctic. The advection of those air masses to Arctic regions took place mainly at altitudes above 1 km. In contrast, observed EC measured by the ALABAMA and rBC from the SP2 have their sources in northern Canada, Europe, and southern North America (Figs. 11b-d, respectively). However, rBC mass concentrations were generally low during the NETCARE 2014 study (Schulz et al., 2019), reflecting the largely isolated

395 nature of the summertime Arctic from the rest of the atmosphere. Finally, nss-nitrate- and EC-containing particles were larger in diameter compared to TMA-containing particles (Fig. S11), consistent with pronounced influences of aerosol processing during long range transport.

Measurements by the HR-ToF-AMS combined with air mass history analysis suggest that long range transport from sources outside the Arctic contributed to the abundance of particles containing sulfate and ammonium. Both species show slightly

400 higher mass concentrations in the Arctic FT during both periods (Fig. 10). In addition, sulfate was predominantly abundant when the residence time prior to sampling was high in East Asia, Europe, and southern North America (Figs. 11a, c, and d, respectively), in line with prior studies (e.g., Breider et al., 2014; Yang et al., 2018). Consistent with findings by Schmale et al. (2011), the sulfate-to-organic ratio in the FT was enhanced with increasing influences from East Asia (Fig. 11a). Finally, sources in Europe, southern North America, and northern Canada contribute to the presence of particles containing ammonium

405 (Figs. 11c, d, and b, respectively). Taken together, aerosol particle composition in the summertime Arctic BL and lower FT was driven by a combination of processes occurring along transport pathways and within Arctic regions, respectively. The
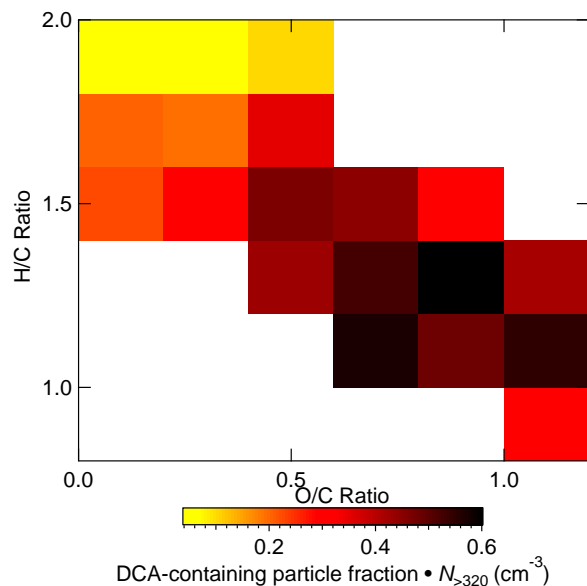
Figure 12. Scaled number concentration ($PF \cdot N_{>320}$) of DCA-containing particles measured by the ALABAMA (colored) as a function of the HR-ToF-AMS estimated oxygen-to-carbon (O/C) and hydrogen-to-carbon (H/C) during the Arctic air mass period. Uncertainty analysis is given in Supplement Sect. 7.
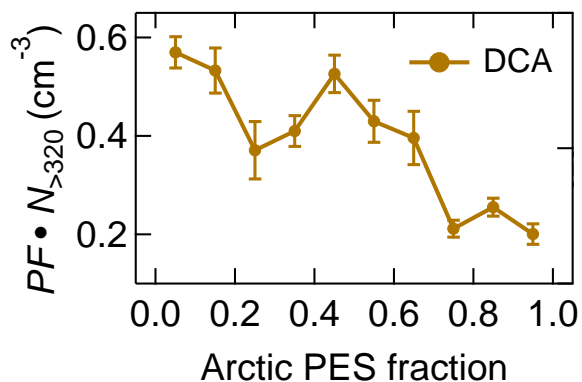
Figure 13. Scaled number concentration ($PF \cdot N_{>320}$) of DCA-containing particles measured by the ALABAMA as a function of FLEXPART derived air mass residence time over Arctic regions during the Arctic air mass period. Uncertainty analysis is given in the Supplement Sect. 7.

following section presents a detailed analysis of the influences from specific aerosol sources at southern latitudes on aerosol particle composition.
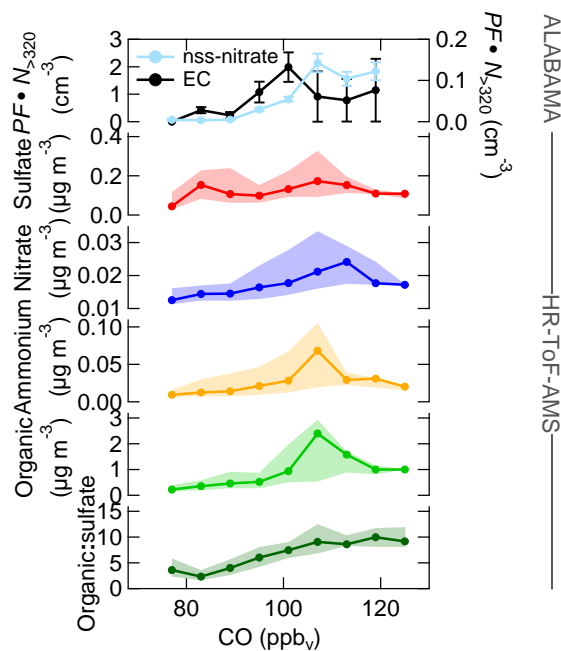
Figure 14. Aerosol composition measured by the ALABAMA and by the HR-ToF-AMS (indicated on the right side) as a function of CO mixing ratios during the southern air mass period. Top panel represents the ALABAMA scaled number concentration ($PF \cdot N_{>320}$) with right axis referring to EC-containing (black) and left axis referring to nss-nitrate-containing (light blue) particles. Lower panels represent each median (solid line with marker) and interquartile ranges (shaded area) of the HR-ToF-AMS mass concentrations of sulfate (red), nitrate (blue), ammonium (orange), organic matter (light green), and the organic-to-sulfate ratio (dark green). Uncertainty analyses are given in the Supplement Sect. 7.

3.5 Vegetation fire and anthropogenic influences on particle composition

410 Anthropogenic and/or vegetation fire emissions contributed largely to the abundance of EC- and nss-nitrate-containing particles in the summertime Arctic FT, particularly during the southern air mass period. To illustrate this, Fig. 14 shows the aerosol composition as a function of CO mixing ratios during the southern air mass period. Additionally, Fig. 15 provide the aerosol composition as a function of FLEXPART derived air mass residence time over vegetation fires, populated, and industrial areas, respectively. The number concentration of nss-nitrate particles measured by the ALABAMA increased with elevated

415 CO mixing ratios (Fig. 14). In parallel, air mass history shows that nss-nitrate particles were largely abundant when time spent over vegetation fires in northern Canada as well as over populated areas was high (Figs. 15a and b). Consistent with these results, nitrate mass concentrations measured by the HR-ToF-AMS also increased with increasing influence from vegetation fires and population (Figs. 15a and b). Similar to nitrate, enhanced sulfate and ammonium concentrations measured by the HR-ToF-AMS coincided with both high CO mixing ratios and with time spent over vegetation fires (Figs. 14 and 15a). Along with

420 vegetation fires and high CO mixing ratios, the organic-to-sulfate ratio was increasing, indicating the pronounced influence of
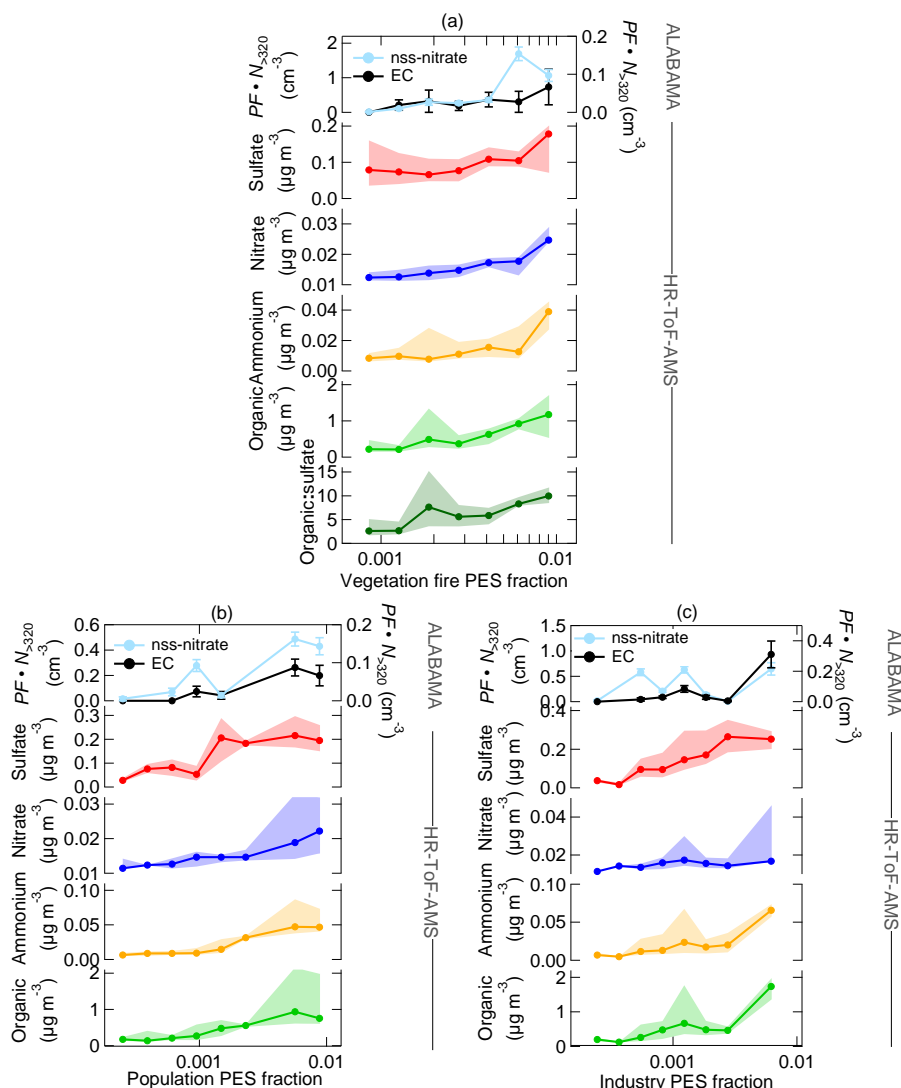
Figure 15. Aerosol composition measured by the ALABAMA and by the HR-ToF-AMS (indicated on the right side) as a function of FLEXPART derived residence time over (a) vegetation fires, (b) populated areas, and (c) industrial areas during the southern air mass period. Top panel represents the ALABAMA scaled number concentration ($PF \cdot N_{>320}$) with right axis referring to EC-containing (black) and left axis referring to nss-nitrate-containing (light blue) particles. Lower panels represent each median (solid line with marker) and interquartile ranges (shaded area) of the HR-ToF-AMS mass concentrations of sulfate (red), nitrate (blue), ammonium (orange), and organic matter (light green) as well as organic-to-sulfate ratio (dark green). Uncertainty analyses are given in the Supplement Sect. 7.

vegetation fire emissions on the presence of organic matter in the summertime Arctic FT.

Contrary to what is expected, measurements by the HR-ToF-AMS during the second period show decreasing concentrations of sulfate, nitrate, ammonium, and organic matter with highest CO mixing ratios (Fig. 14). However, the number fraction of

nss-nitrate-containing particles (Fig. S22) and the organic-to-sulfate ratio (Fig. 14) were increasing with high CO mixing ratios.

425 Along with the low-pressure system (see Sect. 3.1.2), the transport of air masses that were characterized by high CO mixing ratios from vegetation fires in northern Canada (Fig. S36) was accompanied with precipitation events, as can be seen in GFS archive data (wetter3, 2020). It is thus conceivable that this transport pathway was linked to intensive particle wash-out events (Garrett et al., 2010, 2011; Browse et al., 2012).

Enhanced concentrations of nitrate, ammonium, and organic matter as a result of transport from lower latitude sources, mainly

430 from vegetation fires, is consistent with previous observational and modeling studies (Kuhn et al., 2010; Chang et al., 2011; Brock et al., 2011; Breider et al., 2014). Interestingly, the ALABAMA analysis shows no significant evidence of influences from vegetation fires on the abundance of EC particles, contrary to earlier findings (e.g., Hirdman et al., 2010; Bourgeois and Bey, 2011; Stohl et al., 2013; Breider et al., 2014; Sobhani et al., 2018). This result might be explained by the following reasons. It is known from previous field studies that chemically aged BC particles from vegetation fires are thickly coated with organics

435 and inorganics (e.g., Paris et al., 2009; Singh et al., 2010; Kondo et al., 2011; Brock et al., 2011). In addition, a laboratory study by Silva et al. (1999) reported the majority of biomass burning particles to include potassium. Given that potassium is known to produce matrix effects, owing to its low ionization potential (e.g., Silva and Prather, 2000), positive ion signals, other than K^+, in biomass burning particle spectra are likely suppressed by the presence of potassium. Further, Moffet and Prather (2009) reported negative ion mass spectra of aged soot to be dominated by nitrate and sulfate signals. Together, it is likely

440 that signals of carbon cluster ions, indicative for the presence of EC/soot, are suppressed by other substances that are abundant in biomass burning particles. This hypothesis is consistent with previous SPMS measurements during field experiments at southern latitudes characterizing biomass burning aerosol (e.g., Pratt et al., 2011; Zauscher et al., 2013; Gunsch et al., 2018). In detail, mean mass spectra of aged biomass burning particles are generally characterized by the concurrent presence of potassium, sulfate, nitrate, organic acids, and nitrogen-containing organics, confirming findings in our study (see Fig. 7c).

445 However, rBC mass concentration measured by the SP2 (during three out of five flights) provides evidence that vegetation fires in northern Canada contributed to the presence of rBC in the summertime Arctic FT (see Fig. S15). This finding is consistent with recent studies on the summertime Arctic BC burden (Bourgeois and Bey, 2011; Breider et al., 2014; Zhu et al., 2020).

Besides the influence of vegetation fires, the presence of sulfate, ammonium, nitrate, EC, and organic matter in the summertime Arctic FT can further be linked to anthropogenic emissions from southern latitudes. Air mass history illustrates that elevated

450 concentrations of EC particles occurred when the residence time over populated and/or industrial areas in Europe and southern North America was high (compare Figs. 15b-c and S14 with Figs. 11c and d). Consistent with this analysis, the quantitative analysis of rBC by the SP2 shows qualitatively similar trends for the Arctic air mass period (Fig. S14). Particularly during the southern air mass period, enhanced sulfate, ammonium, nitrate, and organic concentrations coincided with time spent over populated and/or industrial areas (Fig. 15b-c).

455 The ALABAMA data show that the presence of EC particles in the Arctic can partly be associated with industrial emissions in southern North America (compare Figs. 15c and 11d), likely including flaring emissions (compare Fig. S34 with Fig. 3b and c). Figure S34 illustrates that long range transport from southern North America to Arctic regions might accompanied by emissions from oil production industry in Alberta, Canada (compare with Fig. 3c). This result is consistent with recent modeling

studies, demonstrating the importance of anthropogenic BC sources in northern Eurasia and North America (e.g., Huang et al.,
460 2010; Bourgeois and Bey, 2011; Sobhani et al., 2018). Particularly, studies by Stohl et al. (2013) and Evangeliou et al. (2018)
demonstrated the importance of distant sources in southern North America to affect the abundance of EC-containing particles in
the Arctic summer. The authors showed that regions in western Canada (Alberta), operating numerous oil producing facilities,
influenced aerosol particle composition in the Arctic summer. However, contributions from sources in South Asia cannot be
confirmed by our measurements, which might be related to maximum sampling altitude up to 3.5 km that is less sensitive to
465 Asian pollution sources (e.g., Bourgeois and Bey, 2011; Sharma et al., 2013; Sobhani et al., 2018).

4 Conclusions

Motivated by the limited knowledge of summertime Arctic aerosol, our study aimed to improve our understanding of sources
impacting the vertical structure of aerosol particle chemical composition. Aircraft-based measurements were performed using
two complementary aerosol mass spectrometers, the ALABAMA and HR-ToF-AMS, and an SP2 in the summertime Canadian
470 Arctic lower troposphere.
Our measurements and air mass trajectory analysis show that the vertical structure of aerosol particle composition in the
summertime Arctic lower troposphere was driven by a combination of aerosol processes occurring along northward transport
pathways and within Arctic regions. In our prior studies, we could show that particle composition in the isolated stable stratified
boundary layer was characterized by the abundance of MSA, sodium, chloride, and organic matter that is partly associated with
475 particulate TMA (Willis et al., 2016, 2017; Köllner et al., 2017). Further, we observed that particulate TMA was externally
mixed from sea spray particles and smaller in diameter, suggesting a role of marine-derived secondary organic aerosol forma-
tion occurring alongside with primary sea-to-air emissions. Here, the presented results confirm the marine source of TMA by
our FLEXPART air mass history analysis. The presence of TMA-containing particles correlated, similar to sea spray particles,
with time spent over Arctic open water regions. Overall, this study together with findings from earlier work on the NETCARE
480 2014 measurements emphasize the importance of marine SOA formation on the vertical structure of particle composition in
the summertime Arctic (Willis et al., 2016, 2017; Köllner et al., 2017; Croft et al., 2019).
As new results compared to our prior studies, we discussed particle composition measured during two distinctive synoptic
situations in the summertime Arctic lower FT, namely the Arctic and the southern air mass periods. In contrast to the isolated
Arctic BL, particle composition aloft was characterized by the presence of nss-nitrate, EC, ammonium, sulfate, and oxidized
485 organics that can partly be attributed to DCA transported long distances from mid-latitude sources. However, particle com-
position in the FT varied with the synoptic situations, owing to different particle sources and transport pathways. Comparing
both periods, the organic, ammonium, and nitrate concentrations measured by HR-ToF-AMS as well as the nitrate fraction by
the ALABAMA were higher during the southern air mass period, reflecting the pronounced influence of vegetation fires in
northern Canada during this time. Our air mass history analysis showed that elevated concentrations of nitrate, ammonium,
490 rBC, and organic matter occurred when the residence time over vegetation fires in northern Canada was high. Further, those
particles were largely present in high CO air masses. Also the organic-to-sulfate ratio coincided with time the air mass spent

over these fires.

Besides the influence of vegetation fires, anthropogenic sources in Europe, North America, and East Asia contributed to the presence of particles containing nitrate, EC, organic matter, ammonium, and sulfate in the summertime Arctic FT. The pres-
495 ence of those particles correlated with time spent over populated and industrial areas in Europe, East Asia, and southern North America. Measurements of enhanced EC concentrations can be traced back to oil production industry, including flaring, in Alberta (Canada), by means of the FLEXPART analysis. Further, particles size of EC and nss-nitrate types were larger compared to TMA-containing particles, suggesting aging processes during long range transport.

Particularly during the first period, our analysis showed that the majority of DCA-containing particles were observed in the
500 Arctic FT and in air masses that spent significant time outside Arctic regions. Long range transport of aerosol and precursors from distant sources thus influenced the abundance of DCA particles in the summertime Arctic FT. These findings add to our understanding of organic acids in summer Arctic aerosol, because previous studies were confined to ground-based and shipborne datasets. Combined with the largely stable stratified nature of the Arctic lower troposphere, previous BL datasets were therefore less sensitive to organic acids from long range transport and related processes.

505 Together, these results indicate the important role of mid-latitude aerosol sources on summertime Arctic particle composition in the lower FT. Particularly, contributions from biomass burning emissions on summertime Arctic aerosol are likely to increase under scenarios for the future climate (e.g., Randerson et al., 2006; de Groot et al., 2013; Marelle et al., 2018; Evangeliou et al., 2019). To our knowledge, this is the first study providing comprehensive particle chemical composition analysis in the summertime Arctic FT, by using two complementary aerosol mass spectrometers with black carbon measurements from an
510 SP2. However, open questions remain, partly owing to limitations of the current study. Being limited by the spatial and temporal range of the NETCARE 2014 measurements, it is difficult to asses the representativeness of the findings for the whole Arctic. Future widespread and long-term measurements would help to extend the results to other Arctic regions and seasons. Lagrangian flight experiments would help to better constrain the relative role of aerosol processing, including wet removal and photochemical aging, on summertime Arctic particle composition. Based on limitations in sampling altitude, future Arctic air-
515 borne measurements in the mid to upper troposphere are necessary to further characterize the impact of mid-latitude pollution sources on summertime Arctic aerosol properties. Finally, it is of relevance to further characterize organic compounds in Arctic aerosol along with their sources, formation processes, and impact on clouds.

Data availability. The ALABAMA and FLEXPART data can be accessed by contacting the corresponding author F. Köllner (f.koellner@mpic.de) or the second author J. Schneider (johannes.schneider@mpic.de). Other NETCARE data presented in this publication are publicly available
520 through the Government of Canada open data portal (https://open.canada.ca).

Author contributions. JA, RL, and AH designed the research project. FK, JS, HB, RL, MW, and JB carried out the measurements. AA processed the AIMMS-20 data. TK, FH, and JS re-designed and further developed the ALABAMA for aircraft-based measurements. DK

provided the FLEXPART output. MW provided the HR-ToF-AMS data. HS provided the SP2 and UHSAS data. HB provided the CO data. FK performed the data analyses with critical feedback from JS, PH, MW, TK, DK, and JA. FK wrote the manuscript. The manuscript was

525   critically reviewed by JS, PH, SB, JA, MW, RL, DK, and HS.

Competing interests.   The authors declare that they have no conflict of interest.

Acknowledgements.   The authors thank Kenn Borek Air Ltd., in particular our pilots Kevin Elke and John Bayes, as well as our aircraft maintenance engineer Kevin Riehl. We thank Jim Hodgson and Lake Central Air Services in Muskoka, Jim Watson (Scale Modelbuilders, Inc.), Julia Binder and Martin Gehrmann (Alfred Wegener Institute, AWI) for their support of the integration of the instrumentation in the

530   aircraft. We thank Bob Christensen (University of Toronto), Lukas Kandora, Manuel Sellmann, Christian Konrad, and Jens Herrmann (AWI), Desiree Toom, Sangeeta Sharma (ECCC), Kathy Law and Jenny Thomas (LATMOS) for their support before and during the study. We thank Christiane Schulz (MPIC) for her support during the integration of the instruments in Muskoka. We thank the Biogeochemistry department of MPIC for providing the CO instrument and Dieter Scharffe for his support during the preparation phase of the campaign. We thank the Nunavut Research Institute and the Nunavut Impact Review Board for licensing the study. Logistical support in Resolute Bay was provided

535   by the Polar Continental Shelf Project (PCSP) of Natural Resources Canada under PCSP Field Project 218-14. Funding for this work was provided by the Natural Sciences and Engineering Research Council of Canada through the NETCARE project of the Climate Change and Atmospheric Research Program, the Alfred Wegener Institute, Environment and Climate Change Canada, and the Max Planck Society. Special thanks to the whole NETCARE-team for data exchange, discussions and support. The authors thank Alexandre Caseiro (MPIC) for his help and discussions on satellite data and for providing the VIIRS nightfire "*Flares Only*" product. We thank Oliver Appel (MPIC) for

540   helpful discussions on data analysis of the ALABAMA instrument.

References

Abbatt, J. P. D., Leaitch, W. R., Aliabadi, A. A., Bertram, A. K., Blanchet, J.-P., Boivin-Rioux, A., Bozem, H., Burkart, J., Chang, R. Y. W., Charette, J., Chaubey, J. P., Christensen, R. J., Cirisan, A., Collins, D. B., Croft, B., Dionne, J., Evans, G. J., Fletcher, C. G., Galí, M., Ghahremaninezhad, R., Girard, E., Gong, W., Gosselin, M., Gourdal, M., Hanna, S. J., Hayashida, H., Herber, A. B., Hesaraki, S., Hoor, P., Huang, L., Hussherr, R., Irish, V. E., Keita, S. A., Kodros, J. K., Köllner, F., Kolonjari, F., Kunkel, D., Ladino, L. A., Law, K., Levasseur, M., Libois, Q., Liggio, J., Lizotte, M., Macdonald, K. M., Mahmood, R., Martin, R. V., Mason, R. H., Miller, L. A., Moravek, A., Mortenson, E., Mungall, E. L., Murphy, J. G., Namazi, M., Norman, A.-L., O'Neill, N. T., Pierce, J. R., Russell, L. M., Schneider, J., Schulz, H., Sharma, S., Si, M., Staebler, R. M., Steiner, N. S., Thomas, J. L., von Salzen, K., Wentzell, J. J. B., Willis, M. D., Wentworth, G. R., Xu, J.-W., and Yakobi-Hancock, J. D.: Overview paper: New insights into aerosol and climate in the Arctic, Atmos. Chem. Phys., 19, 2527–2560, https://doi.org/10.5194/acp-19-2527-2019, 2019.

Aero-Laser GmbH: Ultra-Fast Carbon-Monoxide Analyser AL5002-Manual-Version 1.24, Aero-Laser GmbH, 2013.

Aliabadi, A. A., Staebler, R. M., and Sharma, S.: Air quality monitoring in communities of the Canadian Arctic during the high shipping season with a focus on local and marine pollution, Atmos. Chem. Phys., 15, 2651–2673, https://doi.org/10.5194/acp-15-2651-2015, 2015.

Aliabadi, A. A., Staebler, R., Liu, M., and Herber, A.: Characterization and Parametrization of Reynolds Stress and Turbulent Heat Flux in the Stably-Stratified Lower Arctic Troposphere Using Aircraft Measurements, Bound.-Lay. Meteorol., pp. 1–28, https://doi.org/10.1007/s10546-016-0164-7, 2016a.

Aliabadi, A. A., Thomas, J. L., Herber, A. B., Staebler, R. M., Leaitch, W. R., Schulz, H., Law, K. S., Marelle, L., Burkart, J., Willis, M. D., Bozem, H., Hoor, P. M., Köllner, F., Schneider, J., Levasseur, M., and Abbatt, J. P. D.: Ship emissions measurement in the Arctic by plume intercepts of the Canadian Coast Guard icebreaker *Amundsen* from the *Polar 6* aircraft platform, Atmos. Chem. Phys., 16, 7899–7916, https://doi.org/10.5194/acp-16-7899-2016, 2016b.

AMAP: Assessment 2007: Oil and Gas Activities in the Arctic - Effects and Potential Effects, Arctic Monitoring and Assessment Programme (AMAP), Oslo, Norway, 2, vii + 277, 2010.

Andreae, M. O. and Merlet, P.: Emission of trace gases and aerosols from biomass burning, Global Biogeochem. Cy., 15, 955–966, https://doi.org/10.1029/2000GB001382, 2001.

Angelino, S., Suess, D. T., and Prather, K. A.: Formation of Aerosol Particles from Reactions of Secondary and Tertiary Alkylamines: Characterization by Aerosol Time-of-Flight Mass Spectrometry, Environ. Sci. Technol., 35(15), 3130–3138, https://doi.org/10.1021/es0015444, 2001.

Arnold, S., Law, K., Brock, C., Thomas, J., Starkweather, S., Von Salzen, K., Stohl, A., Sharma, S., Lund, M., Flanner, M., Petäjä, T., Tanimoto, H., Gamble, J., Dibb, J., Melamed, M., Johnson, N., Fidel, M., Tynkkynen, V., Baklanov, A., Eckhardt, S., Monks, S., Browse, J., and Bozem, H.: Arctic air pollution: Challenges and opportunities for the next decade, Elementa, 2016, https://doi.org/10.12952/journal.elementa.000104, 2016.

Aventech: www.aventech.com/products/aimms20.html, last access: 25.05.2018, 2018.

Boucher, O., Randall, D., Artaxo, P., Bretherton, C., Feingold, G., Forster, P., Kerminen, V.-M., Kondo, Y., Liao, H., Lohmann, U., Rasch, P., Satheesh, S., Sherwood, S., Stevens, B., and Zhang, X.: Climate Change 2013: The Physical Science Basis. Contribution of Working Group I to the Fifth Assessment Report of the Intergovernmental Panel on Climate Change, chap. Clouds and Aerosols, pp. 571–658, Cambridge University Press, https://doi.org/DOI: 10.1017/CBO9781107415324.016, 2013.

Bourgeois, Q. and Bey, I.: Pollution transport efficiency toward the Arctic: Sensitivity to aerosol scavenging and source regions, J. Geophys. Res.-Atmos., 116, https://doi.org/10.1029/2010JD015096, 2011.

Bozem, H., Hoor, P., Kunkel, D., Köllner, F., Schneider, J., Herber, A., Schulz, H., Leaitch, W. R., Aliabadi, A. A., Willis, M. D., Burkart, J., and Abbatt, J. P. D.: Characterization of Transport Regimes and the Polar Dome during Arctic Spring and Summer using in-situ Aircraft Measurements, Atmos. Chem. Phys. Discuss., 2019, 1–36, https://doi.org/10.5194/acp-2019-70, 2019.

Brands, M.: Aufbau und Charakterisierung eines fugzeuggetragenen Einzel-partikel-Massenspektrometers, Ph.D. thesis, Johannes-Gutenberg Universität Mainz, 2009.

Brands, M., Kamphus, M., Böttger, T., Schneider, J., Drewnick, F., Roth, A., Curtius, J., Voigt, C., Borbon, A., Beekmann, M., Bourdon, A., Perrin, T., and Borrmann, S.: Characterization of a Newly Developed Aircraft-Based Laser Ablation Aerosol Mass Spectrometer (ALABAMA) and First Field Deployment in Urban Pollution Plumes over Paris During MEGAPOLI 2009, Aerosol Sci. Technol., 45, 46–64, https://doi.org/10.1080/02786826.2010.517813, 2011.

Breider, T. J., Mickley, L. J., Jacob, D. J., Wang, Q., Fisher, J. A., Chang, R. Y.-W., and Alexander, B.: Annual distributions and sources of Arctic aerosol components, aerosol optical depth, and aerosol absorption, J. Geophys. Res.-Atmos., 119, 4107–4124, https://doi.org/10.1002/2013JD020996, 2014.

Brock, C. A., Radke, L. F., Lyons, J. H., and Hobbs, P. V.: Arctic hazes in summer over Greenland and the North American Arctic. I: Incidence and origins, Journal of Atmospheric Chemistry, 9, 129–148, https://doi.org/10.1007/BF00052828, https://doi.org/10.1007/BF00052828, 1989.

Brock, C. A., Cozic, J., Bahreini, R., Froyd, K. D., Middlebrook, A. M., McComiskey, A., Brioude, J., Cooper, O. R., Stohl, A., Aikin, K. C., de Gouw, J. A., Fahey, D. W., Ferrare, R. A., Gao, R.-S., Gore, W., Holloway, J. S., Hübler, G., Jefferson, A., Lack, D. A., Lance, S., Moore, R. H., Murphy, D. M., Nenes, A., Novelli, P. C., Nowak, J. B., Ogren, J. A., Peischl, J., Pierce, R. B., Pilewskie, P., Quinn, P. K., Ryerson, T. B., Schmidt, K. S., Schwarz, J. P., Sodemann, H., Spackman, J. R., Stark, H., Thomson, D. S., Thornberry, T., Veres, P., Watts, L. A., Warneke, C., and Wollny, A. G.: Characteristics, sources, and transport of aerosols measured in spring 2008 during the aerosol, radiation, and cloud processes affecting Arctic Climate (ARCPAC) Project, Atmos. Chem. Phys., 11, 2423–2453, https://doi.org/10.5194/acp-11-2423-2011, 2011.

Browse, J., Carslaw, K. S., Arnold, S. R., Pringle, K., and Boucher, O.: The scavenging processes controlling the seasonal cycle in Arctic sulphate and black carbon aerosol, Atmos. Chem. Phys., 12, 6775–6798, https://doi.org/10.5194/acp-12-6775-2012, 2012.

Burkart, J., Willis, M. D., Bozem, H., Thomas, J. L., Law, K., Hoor, P., Aliabadi, A. A., Köllner, F., Schneider, J., Herber, A., Abbatt, J. P. D., and Leaitch, W. R.: Summertime observations of elevated levels of ultrafine particles in the high Arctic marine boundary layer, Atmos. Chem. Phys., 17, 5515–5535, https://doi.org/10.5194/acp-17-5515-2017, 2017.

Cai, Y., Montague, D. C., Mooiweer-Bryan, W., and Deshler, T.: Performance characteristics of the ultra high sensitivity aerosol spectrometer for particles between 55 and 800 nm: Laboratory and field studies, J. Aerosol Sci., 39, 759 – 769, https://doi.org/10.1016/j.jaerosci.2008.04.007, 2008.

Cavalieri, D. J., Parkinson, C. L., Gloersen, P., and Zwally, H. J.: Sea Ice Concentrations from Nimbus-7 SMMR and DMSP SSM/I-SSMIS Passive Microwave Data, Version 1, NSIDC-0051, Boulder, Colorado USA. NASA National Snow and Ice Data Center Distributed Active Archive Center, https://doi.org/https://doi.org/10.5067/8GQ8LZQVL0VL, last access: 08.06.2018, 1996, updated yearly.

Chang, R. Y.-W., Leck, C., Graus, M., Müller, M., Paatero, J., Burkhart, J. F., Stohl, A., Orr, L. H., Hayden, K., Li, S.-M., Hansel, A., Tjernström, M., Leaitch, W. R., and Abbatt, J. P. D.: Aerosol composition and sources in the central Arctic Ocean during ASCOS, Atmos. Chem. Phys., 11, 10 619–10 636, https://doi.org/10.5194/acp-11-10619-2011, 2011.

615   Creamean, J. M., Maahn, M., de Boer, G., McComiskey, A., Sedlacek, A. J., and Feng, Y.: The influence of local oil exploration and regional wildfires on summer 2015 aerosol over the North Slope of Alaska, Atmos. Chem. Phys., 18, 555–570, https://doi.org/10.5194/acp-18-555-2018, 2018.

Croft, B., Martin, R. V., Leaitch, W. R., Burkart, J., Chang, R. Y.-W., Collins, D. B., Hayes, P. L., Hodshire, A. L., Huang, L., Kodros, J. K., Moravek, A., Mungall, E. L., Murphy, J. G., Sharma, S., Tremblay, S., Wentworth, G. R., Willis, M. D., Abbatt, J. P. D., and Pierce,

620   J. R.: Arctic marine secondary organic aerosol contributes significantly to summertime particle size distributions in the Canadian Arctic Archipela-go, Atmos. Chem. Phys., 2019, 2787–2812, https://doi.org/10.5194/acp-19-2787-2019, 2019.

Curry, J. A., Schramm, J. L., and Ebert, E. E.: Sea Ice-Albedo Climate Feedback Mechanism, J. Climate, 8, 240–247, https://doi.org/10.1175/1520-0442(1995)008<0240:SIACFM>2.0.CO;2, 1995.

de Groot, W. J., Flannigan, M. D., and Cantin, A. S.: Climate change impacts on future boreal fire regimes, Forest Ecology and Management,

625   294, 35–44, https://doi.org/10.1016/j.foreco.2012.09.027, 2013.

DeCarlo, P. F., Kimmel, J. R., Trimborn, A., Northway, M. J., Jayne, J. T., Aiken, A. C., Gonin, M., Fuhrer, K., Horvath, T., Docherty, K. S., Worsnop, D. R., and Jimenez, J. L.: Field-Deployable, High-Resolution, Time-of-Flight Aerosol Mass Spectrometer, Anal. Chem., 78, 8281–8289, https://doi.org/10.1021/ac061249n, 2006.

Eckhardt, S., Hermansen, O., Grythe, H., Fiebig, M., Stebel, K., Cassiani, M., Baecklund, A., and Stohl, A.: The influence of

630   cruise ship emissions on air pollution in Svalbard - a harbinger of a more polluted Arctic?, Atmos. Chem. Phys., 13, 8401–8409, https://doi.org/10.5194/acp-13-8401-2013, 2013.

Elvidge, C. D., Zhizhin, M., Hsu, F.-C., and Baugh, K. E.: VIIRS Nightfire: Satellite Pyrometry at Night, Remote Sensing, 5, 4423–4449, https://doi.org/10.3390/rs5094423, 2013.

Elvidge, C. D., Zhizhin, M., Baugh, K., Hsu, F.-C., and Ghosh, T.: Methods for Global Survey of Natural Gas Flaring from Visible Infrared

635   Imaging Radiometer Suite Data, Energies, 9, https://doi.org/10.3390/en9010014, 2016.

Evangeliou, N., Thompson, R. L., Eckhardt, S., and Stohl, A.: Top-down estimates of black carbon emissions at high latitudes using an atmospheric transport model and a Bayesian inversion framework, Atmos. Chem. Phys., 18, 15 307–15 327, https://doi.org/10.5194/acp-18-15307-2018, 2018.

Evangeliou, N., Kylling, A., Eckhardt, S., Myroniuk, V., Stebel, K., Paugam, R., Zibtsev, S., and Stohl, A.: Open fires in Greenland

640   in summer 2017: transport, deposition and radiative effects of BC, OC and BrC emissions, Atmos. Chem. Phys., 19, 1393–1411, https://doi.org/10.5194/acp-19-1393-2019, 2019.

Ferrero, L., Cappelletti, D., Busetto, M., Mazzola, M., Lupi, A., Lanconelli, C., Becagli, S., Traversi, R., Caiazzo, L., Giardi, F., Moroni, B., Crocchianti, S., Fierz, M., Močnik, G., Sangiorgi, G., Perrone, M. G., Maturilli, M., Vitale, V., Udisti, R., and Bolzacchini, E.: Vertical profiles of aerosol and black carbon in the Arctic: a seasonal phenomenology along 2 years (2011–2012) of field campaigns, Atmos.

645   Chem. Phys., 16, 12 601–12 629, https://doi.org/10.5194/acp-16-12601-2016, 2016.

Flanner, M. G., Shell, K. M., Barlage, M., Perovich, D. K., and Tschudi, M. A.: Radiative forcing and albedo feedback from the Northern Hemisphere cryosphere between 1979 and 2008, Nature Geoscience, 4, 151–155, https://doi.org/10.1038/ngeo1062, 2011.

Froyd, K. D., Murphy, D. M., Brock, C. A., Campuzano-Jost, P., Dibb, J. E., Jimenez, J.-L., Kupc, A., Middlebrook, A. M., Schill, G. P., Thornhill, K. L., Williamson, C. J., Wilson, J. C., and Ziemba, L. D.: A new method to quantify mineral dust and other

650   aerosol species from aircraft platforms using single-particle mass spectrometry, Atmospheric Measurement Techniques, 12, 6209–6239, https://doi.org/10.5194/amt-12-6209-2019, https://www.atmos-meas-tech.net/12/6209/2019/, 2019.

Fu, P., Kawamura, K., Chen, J., and Barrie, L. A.: Isoprene, Monoterpene, and Sesquiterpene Oxidation Products in the High Arctic Aerosols during Late Winter to Early Summer, Environ. Sci. Technol., 43, 4022–4028, https://doi.org/10.1021/es803669a, 2009.

Fu, P., Kawamura, K., Usukura, K., and Miura, K.: Dicarboxylic acids, ketocarboxylic acids and glyoxal in the marine aerosols collected during a round-the-world cruise, Mar. Chem., 148, 22 – 32, https://doi.org/10.1016/j.marchem.2012.11.002, 2013.

Fuelberg, H. E., Harrigan, D. L., and Sessions, W.: A meteorological overview of the ARCTAS 2008 mission, Atmos. Chem. Phys., 10, 817–842, https://doi.org/10.5194/acp-10-817-2010, 2010.

Gao, R. S., Schwarz, J. P., Kelly, K. K., Fahey, D. W., Watts, L. A., Thompson, T. L., Spackman, J. R., Slowik, J. G., Cross, E. S., Han, J.-H., Davidovits, P., Onasch, T. B., and Worsnop, D. R.: A Novel Method for Estimating Light-Scattering Properties of Soot Aerosols Using a Modified Single-Particle Soot Photometer, Aerosol Sci. Technol., 41, 125–135, https://doi.org/10.1080/02786820601118398, 2007.

Garrett, T., Zhao, C., and Novelli, P.: Assessing the relative contributions of transport efficiency and scavenging to seasonal variability in Arctic aerosol, Tellus B, 62, 190–196, https://doi.org/10.1111/j.1600-0889.2010.00453.x, 2010.

Garrett, T. J., Brattström, S., Sharma, S., Worthy, D. E. J., and Novelli, P.: The role of scavenging in the seasonal transport of black carbon and sulfate to the Arctic, Geophysical Research Letters, 38, https://doi.org/10.1029/2011GL048221, https://agupubs.onlinelibrary.wiley.com/doi/abs/10.1029/2011GL048221, 2011.

Guasco, T. L., Cuadra-Rodriguez, L. A., Pedler, B. E., Ault, A. P., Collins, D. B., Zhao, D., Kim, M. J., Ruppel, M. J., Wilson, S. C., Pomeroy, R. S., Grassian, V. H., Azam, F., Bertram, T. H., and Prather, K. A.: Transition Metal Associations with Primary Biological Particles in Sea Spray Aerosol Generated in a Wave Channel, Environ. Sci. Technol., 48, 1324–1333, https://doi.org/10.1021/es403203d, 2014.

Gunsch, M. J., Kirpes, R. M., Kolesar, K. R., Barrett, T. E., China, S., Sheesley, R. J., Laskin, A., Wiedensohler, A., Tuch, T., and Pratt, K. A.: Contributions of transported Prudhoe Bay oil field emissions to the aerosol population in Utqiaġvik, Alaska, Atmos. Chem. Phys., 17, 10 879–10 892, https://doi.org/10.5194/acp-17-10879-2017, 2017.

Gunsch, M. J., May, N. W., Wen, M., Bottenus, C. L. H., Gardner, D. J., VanReken, T. M., Bertman, S. B., Hopke, P. K., Ault, A. P., and Pratt, K. A.: Ubiquitous influence of wildfire emissions and secondary organic aerosol on summertime atmospheric aerosol in the forested Great Lakes region, Atmos. Chem. Phys., 18, 3701–3715, https://doi.org/10.5194/acp-18-3701-2018, 2018.

Hansen, A. M. K., Kristensen, K., Nguyen, Q. T., Zare, A., Cozzi, F., Nøjgaard, J. K., Skov, H., Brandt, J., Christensen, J. H., Ström, J., Tunved, P., Krejci, R., and Glasius, M.: Organosulfates and organic acids in Arctic aerosols: speciation, annual variation and concentration levels, Atmos. Chem. Phys., 14, 7807–7823, https://doi.org/10.5194/acp-14-7807-2014, 2014.

Haywood, J. and Boucher, O.: Estimates of the direct and indirect radiative forcing due to tropospheric aerosols: A review, Rev. Geophys., 38, 513–543, https://doi.org/10.1029/1999RG000078, 2000.

Healy, R. M., Sciare, J., Poulain, L., Crippa, M., Wiedensohler, A., Prévôt, A. S. H., Baltensperger, U., Sarda-Estève, R., McGuire, M. L., Jeong, C.-H., McGillicuddy, E., O'Connor, I. P., Sodeau, J. R., Evans, G. J., and Wenger, J. C.: Quantitative determination of carbonaceous particle mixing state in Paris using single-particle mass spectrometer and aerosol mass spectrometer measurements, Atmos. Chem. Phys., 13, 9479–9496, https://doi.org/10.5194/acp-13-9479-2013, 2013.

Healy, R. M., Evans, G. J., Murphy, M., Sierau, B., Arndt, J., McGillicuddy, E., O'Connor, I. P., Sodeau, J. R., and Wenger, J. C.: Single-particle speciation of alkylamines in ambient aerosol at five European sites, Anal. Bioanal. Chem., 407, 5899–5909, https://doi.org/10.1007/s00216-014-8092-1, 2015.

Herber, A. B., Dethloff, K., Haas, C., Steinhage, D., Strapp, J. W., Bottenheim, J., McElroy, T., and Yamanouchi, T.: POLAR 5 - a new research aircraft for improved access to the Arctic, ISAR-1, Drastic Change under the Global Warming, Extended Abstract, 2008.

Hirdman, D., Sodemann, H., Eckhardt, S., Burkhart, J. F., Jefferson, A., Mefford, T., Quinn, P. K., Sharma, S., Ström, J., and Stohl, A.:
Source identification of short-lived air pollutants in the Arctic using statistical analysis of measurement data and particle dispersion model
output, Atmos. Chem. Phys., 10, 669–693, https://doi.org/10.5194/acp-10-669-2010, 2010.

Hoffmann, E. H., Tilgner, A., Schrödner, R., Bräuer, P., Wolke, R., and Herrmann, H.: An advanced modeling study on the impacts and
atmospheric implications of multiphase dimethyl sulfide chemistry, Proceedings of the National Academy of Sciences, 113, 11 776–
11 781, https://doi.org/10.1073/pnas.1606320113, https://www.pnas.org/content/113/42/11776, 2016.

Holland, M. M. and Bitz, C. M.: Polar amplification of climate change in coupled models, Climate Dyn., 21, 221–232,
https://doi.org/10.1007/s00382-003-0332-6, 2003.

Huang, L., Gong, S. L., Jia, C. Q., and Lavoué, D.: Relative contributions of anthropogenic emissions to black carbon aerosol in the Arctic,
J. Geophys. Res.-A, 115, https://doi.org/10.1029/2009JD013592, 2010.

IPCC: Climate Change 2014: Synthesis Report. Contribution of Working Groups I, II and III to the Fifth Assessment Report of the Inter-
governmental Panel on Climate Change [Core Writing Team, R.K. Pachauri and L.A. Meyer (eds.)]. IPCC, Geneva, Switzerland, 151 pp.,
2014.

IPPC: Summary for Policymakers. In: Global Warming of 1.5°C. An IPCC Special Report on the impacts of global warming of 1.5°C above
pre-industrial levels and related global greenhouse gas emission pathways, in the context of strengthening the global response to the threat
of climate change, sustainable development, and efforts to eradicate poverty [Masson-Delmotte, V., P. Zhai, H.-O. Pörtner, D. Roberts, J.
Skea, P.R. Shukla, A. Pirani, W. Moufouma-Okia, C. Péan, R. Pidcock, S. Connors, J.B.R. Matthews, Y. Chen, X. Zhou, M.I. Gomis, E.
Lonnoy, T. Maycock, M. Tignor, and T. Waterfield (eds.)]. World Meteorological Organization, Geneva, Switzerland, 32 pp., 2018.

Kane, D. B., Oktem, B., and Johnston, M. V.: Nanoparticle Detection by Aerosol Mass Spectrometry, Aerosol Sci. Technol., 34, 520–527,
https://doi.org/10.1080/02786820117085, 2001.

Kawamura, K. and Bikkina, S.: A review of dicarboxylic acids and related compounds in atmospheric aerosols: Molecular distributions,
sources and transformation, Atmos. Res., 170, 140 – 160, https://doi.org/10.1016/j.atmosres.2015.11.018, 2016.

Kawamura, K., Kasukabe, H., and Barrie, L. A.: Source and reaction pathways of dicarboxylic acids, ketoacids and dicarbonyls in arctic
aerosols: One year of observations, Atmos. Environ., 30, 1709 – 1722, http://dx.doi.org/10.1016/1352-2310(95)00395-9, 1996.

Kawamura, K., Kasukabe, H., and Barrie, L. A.: Secondary formation of water-soluble organic acids and α-dicarbonyls and their con-
tributions to total carbon and water-soluble organic carbon: Photochemical aging of organic aerosols in the Arctic spring, J. Geophys.
Res.-Atmos., 115, https://doi.org/10.1029/2010JD014299, 2010.

Kawamura, K., Ono, K., Tachibana, E., Charriére, B., and Sempéré, R.: Distributions of low molecular weight dicarboxylic acids, ke-
toacids and α-dicarbonyls in the marine aerosols collected over the Arctic Ocean during late summer, Biogeosciences, 9, 4725–4737,
https://doi.org/10.5194/bg-9-4725-2012, 2012.

Kerminen, V.-M., Teinilä, K., Hillamo, R., and Mäkelä, T.: Size-segregated chemistry of particulate dicarboxylic acids in the Arctic atmo-
sphere, Atmos. Environ., 33, 2089 – 2100, https://doi.org/10.1016/S1352-2310(98)00350-1, 1999.

Kirpes, R. M., Bondy, A. L., Bonanno, D., Moffet, R. C., Wang, B., Laskin, A., Ault, A. P., and Pratt, K. A.: Secondary sulfate is internally
mixed with sea spray aerosol and organic aerosol in the winter Arctic, Atmos. Chem. Phys., 18, 3937–3949, https://doi.org/10.5194/acp-
18-3937-2018, 2018.

Klonecki, A., Hess, P., Emmons, L., Smith, L., Orlando, J., and Blake, D.: Seasonal changes in the transport of pollutants into the Arctic
troposphere-model study, J. Geophys. Res.-Atmos., 108, https://doi.org/10.1029/2002JD002199, 8367, 2003.

Köllner, F., Schneider, J., Willis, M. D., Klimach, T., Helleis, F., Bozem, H., Kunkel, D., Hoor, P., Burkart, J., Leaitch, W. R., Aliabadi, A. A., Abbatt, J. P. D., Herber, A. B., and Borrmann, S.: Particulate trimethylamine in the summertime Canadian high Arctic lower troposphere, Atmos. Chem. Phys., 17, 13 747–13 766, https://doi.org/10.5194/acp-17-13747-2017, 2017.

Kondo, Y., Matsui, H., Moteki, N., Sahu, L., Takegawa, N., Kajino, M., Zhao, Y., Cubison, M. J., Jimenez, J. L., Vay, S., Diskin, G. S., Anderson, B., Wisthaler, A., Mikoviny, T., Fuelberg, H. E., Blake, D. R., Huey, G., Weinheimer, A. J., Knapp, D. J., and Brune, W. H.: Emissions of black carbon, organic, and inorganic aerosols from biomass burning in North America and Asia in 2008, J. Geophys. Res.-Atmos., 116, https://doi.org/10.1029/2010JD015152, 2011.

Kuhn, T., Damoah, R., Bacak, A., and Sloan, J. J.: Characterising aerosol transport into the Canadian High Arctic using aerosol mass spectrometry and Lagrangian modelling, Atmos. Chem. Phys., 10, 10 489–10 502, https://doi.org/10.5194/acp-10-10489-2010, 2010.

Kupiszewski, P., Leck, C., Tjernström, M., Sjogren, S., Sedlar, J., Graus, M., Müller, M., Brooks, B., Swietlicki, E., Norris, S., and Hansel, A.: Vertical profiling of aerosol particles and trace gases over the central Arctic Ocean during summer, Atmos. Chem. Phys., 13, 12 405–12 431, https://doi.org/10.5194/acp-13-12405-2013, 2013.

Lange, R., Dall'Osto, M., Skov, H., Nøjgaard, J., Nielsen, I., Beddows, D., Simo, R., Harrison, R., and Massling, A.: Characterization of distinct Arctic aerosol accumulation modes and their sources, Atmos. Environ., 183, 1–10, https://doi.org/10.1016/j.atmosenv.2018.03.060, 2018.

Lathem, T. L., Beyersdorf, A. J., Thornhill, K. L., Winstead, E. L., Cubison, M. J., Hecobian, A., Jimenez, J. L., Weber, R. J., Anderson, B. E., and Nenes, A.: Analysis of CCN activity of Arctic aerosol and Canadian biomass burning during summer 2008, Atmos. Chem. Phys., 13, 2735–2756, https://doi.org/10.5194/acp-13-2735-2013, 2013.

Law, K. S., Stohl, A., Quinn, P. K., Brock, C. A., Burkhart, J. F., Paris, J.-D., Ancellet, G., Singh, H. B., Roiger, A., Schlager, H., Dibb, J., Jacob, D. J., Arnold, S. R., Pelon, J., and Thomas, J. L.: Arctic Air Pollution: New Insights from POLARCAT-IPY, B. Am. Meteorol. Soc., 95, 1873–1895, https://doi.org/10.1175/BAMS-D-13-00017.1, 2014.

Leaitch, W. R., Korolev, A., Aliabadi, A. A., Burkart, J., Willis, M. D., Abbatt, J. P. D., Bozem, H., Hoor, P., Köllner, F., Schneider, J., Herber, A., Konrad, C., and Brauner, R.: Effects of 20–100 nm particles on liquid clouds in the clean summertime Arctic, Atmos. Chem. Phys., 16, 11 107–11 124, https://doi.org/10.5194/acp-16-11107-2016, 2016.

Leaitch, W. R., Russell, L. M., Liu, J., Kolonjari, F., Toom, D., Huang, L., Sharma, S., Chivulescu, A., Veber, D., and Zhang, W.: Organic functional groups in the submicron aerosol at 82.5° N, 62.5° W from 2012 to 2014, Atmos. Chem. Phys., 18, 3269–3287, https://doi.org/10.5194/acp-18-3269-2018, 2018.

Lee, S.-H., Murphy, D. M., Thomson, D. S., and Middlebrook, A. M.: Nitrate and oxidized organic ions in single particle mass spectra during the 1999 Atlanta Supersite Project, J. Geophys. Res.-Atmos, 108, https://doi.org/10.1029/2001JD001455, 8471, 2003.

Liu, D., Quennehen, B., Darbyshire, E., Allan, J. D., Williams, P. I., Taylor, J. W., Bauguitte, S. J.-B., Flynn, M. J., Lowe, D., Gallagher, M. W., Bower, K. N., Choularton, T. W., and Coe, H.: The importance of Asia as a source of black carbon to the European Arctic during springtime 2013, Atmos. Chem. Phys., 15, 11 537–11 555, https://doi.org/10.5194/acp-15-11537-2015, 2015.

Liu, P., Ziemann, P. J., Kittelson, D. B., and McMurry, P. H.: Generating Particle Beams of Controlled Dimensions and Divergence: I. Theory of Particle Motion in Aerodynamic Lenses and Nozzle Expansions, Aerosol Sci. Technol., 22, 293–313, https://doi.org/10.1080/02786829408959748, 1995a.

Liu, P., Ziemann, P. J., Kittelson, D. B., and McMurry, P. H.: Generating Particle Beams of Controlled Dimensions and Divergence: II. Experimental Evaluation of Particle Motion in Aerodynamic Lenses and Nozzle Expansions, Aerosol Sci. Technol., 22, 314–324, https://doi.org/10.1080/02786829408959749, 1995b.

Liu, P. S. K., Deng, R., Smith, K. A., Williams, L. R., Jayne, J. T., Canagaratna, M. R., Moore, K., Onasch, T. B., Worsnop, D. R., and Deshler,
765 T.: Transmission Efficiency of an Aerodynamic Focusing Lens System: Comparison of Model Calculations and Laboratory Measurements
 for the Aerodyne Aerosol Mass Spectrometer, Aerosol Sci. Technol., 41, 721–733, https://doi.org/10.1080/02786820701422278, 2007.

Liu, Y., Hu, C., Zhan, W., Sun, C., Murch, B., and Ma, L.: Identifying industrial heat sources using time-series of the VIIRS Nightfire product
 with an object-oriented approach, Remote Sens. Environ., 204, 347 – 365, https://doi.org/10.1016/j.rse.2017.10.019, 2018.

Marelle, L., Raut, J.-C., Law, K. S., and Duclaux, O.: Current and Future Arctic Aerosols and Ozone From Remote Emissions and
770 Emerging Local Sources - Modeled Source Contributions and Radiative Effects, J. Geophys. Res.-Atmos., 123, 12,942–12,963,
 https://doi.org/10.1029/2018JD028863, 2018.

MaxMind: https://www.maxmind.com/en/free-world-cities-database, last access: 10.06.2018, 2018.

Moffet, R. C. and Prather, K. A.: In-situ measurements of the mixing state and optical properties of soot with implications for radiative
 forcing estimates, P. Natl. Acad. Sci., 106, 11 872–11 877, https://doi.org/10.1073/pnas.0900040106, 2009.

775 Molleker, S., Helleis, F., Klimach, T., Appel, O., Clemen, H.-C., Dragoneas, A., Gurk, C., Hünig, A., Köllner, F., Rubach, F., Schulz, C.,
 Schneider, J., and Borrmann, S.: Application of an O-ring pinch device as a constant pressure inlet (CPI) for airborne sampling, Atmo-
 spheric Measurement Techniques Discussions, 2020, 1–13, https://doi.org/10.5194/amt-2020-66, https://www.atmos-meas-tech-discuss.
 net/amt-2020-66/, 2020.

Neubauer, K. R., Johnston, M. V., and Wexler, A. S.: Humidity effects on the mass spectra of single aerosol particles, Atmos. Environ., 32,
780 2521–2529, https://doi.org/10.1016/S1352-2310(98)00005-3, 1998.

Paris, J.-D., Stohl, A., Nédélec, P., Arshinov, M. Y., Panchenko, M. V., Shmargunov, V. P., Law, K. S., Belan, B. D., and Ciais, P.: Wildfire
 smoke in the Siberian Arctic in summer: source characterization and plume evolution from airborne measurements, Atmos. Chem. Phys.,
 9, 9315–9327, https://doi.org/10.5194/acp-9-9315-2009, 2009.

Pithan, F. and Mauritsen, T.: Arctic amplification dominated by temperature feedbacks in contemporary climate models, Nature Geoscience,
785 7, 181–184, https://doi.org/10.1038/ngeo2071, https://doi.org/10.1038/ngeo2071, 2014.

Prather, K. A., Bertram, T. H., Grassian, V. H., Deane, G. B., Stokes, M. D., DeMott, P. J., Aluwihare, L. I., Palenik, B. P., Azam, F.,
 Seinfeld, J. H., Moffet, R. C., Molina, M. J., Cappa, C. D., Geiger, F. M., Roberts, G. C., Russell, L. M., Ault, A. P., Baltrusaitis,
 J., Collins, D. B., Corrigan, C. E., Cuadra-Rodriguez, L. A., Ebben, C. J., Forestieri, S. D., Guasco, T. L., Hersey, S. P., Kim, M. J.,
 Lambert, W. F., Modini, R. L., Mui, W., Pedler, B. E., Ruppel, M. J., Ryder, O. S., Schoepp, N. G., Sullivan, R. C., and Zhao, D.:
790 Bringing the ocean into the laboratory to probe the chemical complexity of sea spray aerosol, P. Natl. Acad. Sci., 110, 7550–7555,
 https://doi.org/10.1073/pnas.1300262110, 2013.

Pratt, K. A., Murphy, S. M., Subramanian, R., DeMott, P. J., Kok, G. L., Campos, T., Rogers, D. C., Prenni, A. J., Heymsfield, A. J., Seinfeld,
 J. H., and Prather, K. A.: Flight-based chemical characterization of biomass burning aerosols within two prescribed burn smoke plumes,
 Atmos. Chem. Phys., 11, 12 549–12 565, https://doi.org/10.5194/acp-11-12549-2011, 2011.

795 Qin, X., Bhave, P. V., and Prather, K. A.: Comparison of Two Methods for Obtaining Quantitative Mass Concentrations from Aerosol
 Time-of-Flight Mass Spectrometry Measurements, Anal. Chem., 78, 6169–6178, https://doi.org/10.1021/ac060395q, 2006.

Quennehen, B., Schwarzenboeck, A., Schmale, J., Schneider, J., Sodemann, H., Stohl, A., Ancellet, G., Crumeyrolle, S., and Law, K. S.:
 Physical and chemical properties of pollution aerosol particles transported from North America to Greenland as measured during the
 POLARCAT summer campaign, Atmos. Chem. Phys., 11, 10 947–10 963, https://doi.org/10.5194/acp-11-10947-2011, 2011.

800 Radke, L. F. and Hobbs, P. V.: Arctic hazes in summer over Greenland and the North American Arctic. III: A contribution from the natural
 burning of carbonaceous materials and pyrites, J. Atmos. Chem., 9, 161–167, https://doi.org/10.1007/BF00052830, 1989.

Randerson, J. T., Liu, H., Flanner, M. G., Chambers, S. D., Jin, Y., Hess, P. G., Pfister, G., Mack, M. C., Treseder, K. K., Welp, L. R., Chapin, F. S., Harden, J. W., Goulden, M. L., Lyons, E., Neff, J. C., Schuur, E. A. G., and Zender, C. S.: The Impact of Boreal Forest Fire on Climate Warming, Science, 314, 1130–1132, https://doi.org/10.1126/science.1132075, 2006.

805 Rehbein, P. J. G., Jeong, C.-H., McGuire, M. L., Yao, X., Corbin, J. C., and Evans, G. J.: Cloud and Fog Processing Enhanced Gas-to-Particle Partitioning of Trimethylamine, Environ. Sci. Technol., 45, 4346–4352, https://doi.org/10.1021/es1042113, 2011.

Roth, A., Schneider, J., Klimach, T., Mertes, S., van Pinxteren, D., Herrmann, H., and Borrmann, S.: Aerosol properties, source identification, and cloud processing in orographic clouds measured by single particle mass spectrometry on a central European mountain site during HCCT-2010, Atmos. Chem. Phys., 16, 505–524, https://doi.org/10.5194/acp-16-505-2016, 2016.

810 Sand, M., Berntsen, T. K., von Salzen, K., Flanner, M. G., Langner, J., and Victor, D. G.: Response of Arctic temperature to changes in emissions of short-lived climate forcers, Nat. Clim. Change, 6, 286–289, http://dx.doi.org/10.1038/nclimate2880, 2016.

Scharffe, D., Slemr, F., Brenninkmeijer, C. A. M., and Zahn, A.: Carbon monoxide measurements onboard the CARIBIC passenger aircraft using UV resonance fluorescence, Atmos. Meas. Tech., 5, 1753–1760, https://doi.org/10.5194/amt-5-1753-2012, 2012.

Schmale, J., Schneider, J., Ancellet, G., Quennehen, B., Stohl, A., Sodemann, H., Burkhart, J. F., Hamburger, T., Arnold, S. R., 815 Schwarzenboeck, A., Borrmann, S., and Law, K. S.: Source identification and airborne chemical characterisation of aerosol pollution from long-range transport over Greenland during POLARCAT summer campaign 2008, Atmos. Chem. Phys., 11, 10 097–10 123, https://doi.org/10.5194/acp-11-10097-2011, 2011.

Schmidt, S., Schneider, J., Klimach, T., Mertes, S., Schenk, L. P., Kupiszewski, P., Curtius, J., and Borrmann, S.: Online single particle analysis of ice particle residuals from mountain-top mixed-phase clouds using laboratory derived particle type assignment, Atmos. Chem. 820 Phys., 17, 575–594, https://doi.org/10.5194/acp-17-575-2017, 2017.

Schroeder, W. and Giglio, L.: NASA VIIRS Land Science Investigator Processing System (SIPS) Visible Infrared Imaging Radiometer Suite (VIIRS) 375 m & 750 m Active Fire Products: Product User's Guide Version 1.4, Tech. rep., Department of Geographical Sciences, University of Maryland, 2018.

Schroeder, W., Oliva, P., Giglio, L., and Csiszar, I. A.: The New VIIRS 375m active fire detection data product: Algorithm description and 825 initial assessment, Remote Sens. Environ., 143, 85 – 96, https://doi.org/10.1016/j.rse.2013.12.008, 2014.

Schulz, H., Zanatta, M., Bozem, H., Leaitch, W. R., Herber, A. B., Burkart, J., Willis, M. D., Kunkel, D., Hoor, P. M., Abbatt, J. P. D., and Gerdes, R.: High Arctic aircraft measurements characterising black carbon vertical variability in spring and summer, Atmos. Chem. Phys., 2019, 2361–2384, https://doi.org/10.5194/acp-19-2361-2019, 2019.

Schwarz, J. P., Gao, R. S., Fahey, D. W., Thomson, D. S., Watts, L. A., Wilson, J. C., Reeves, J. M., Darbeheshti, M., Baumgardner, D. G., 830 Kok, G. L., Chung, S. H., Schulz, M., Hendricks, J., Lauer, A., Kärcher, B., Slowik, J. G., Rosenlof, K. H., Thompson, T. L., Langford, A. O., Loewenstein, M., and Aikin, K. C.: Single-particle measurements of midlatitude black carbon and light-scattering aerosols from the boundary layer to the lower stratosphere, J. Geophys. Res.-Atmos., 111, https://doi.org/10.1029/2006JD007076, 2006.

Seibert, P. and Frank, A.: Source-receptor matrix calculation with a Lagrangian particle dispersion model in backward mode, Atmos. Chem. Phys., 4, 51–63, https://doi.org/10.5194/acp-4-51-2004, 2004.

835 Serreze, M. C. and Barry, R. G.: Processes and impacts of Arctic amplification: A research synthesis, Global Planet. Change, 77, 85 – 96, https://doi.org/https://doi.org/10.1016/j.gloplacha.2011.03.004, 2011.

Serreze, M. C. and Francis, J. A.: The Arctic Amplification Debate, Climatic Change, 76, 241–264, https://doi.org/10.1007/s10584-005-9017-y, 2006.

Serreze, M. C., Barrett, A. P., Stroeve, J. C., Kindig, D. N., and Holland, M. M.: The emergence of surface-based Arctic amplification, The
840   Cryosphere, 3, 11–19, https://doi.org/10.5194/tc-3-11-2009, 2009.

Sharma, S., Ishizawa, M., Chan, D., Lavoué, D., Andrews, E., Eleftheriadis, K., and Maksyutov, S.: 16-year simulation of Arctic black carbon: Transport, source contribution, and sensitivity analysis on deposition, J. Geophys. Res.-Atmos., 118, 943–964, https://doi.org/10.1029/2012JD017774, 2013.

Shaw, P. M., Russell, L. M., Jefferson, A., and Quinn, P. K.: Arctic organic aerosol measurements show particles from mixed combustion in
845   spring haze and from frost flowers in winter, Geophysical Research Letters, 37, https://doi.org/10.1029/2010GL042831, https://agupubs. onlinelibrary.wiley.com/doi/abs/10.1029/2010GL042831, 2010.

Shindell, D. T., Chin, M., Dentener, F., Doherty, R. M., Faluvegi, G., Fiore, A. M., Hess, P., Koch, D. M., MacKenzie, I. A., Sanderson, M. G., Schultz, M. G., Schulz, M., Stevenson, D. S., Teich, H., Textor, C., Wild, O., Bergmann, D. J., Bey, I., Bian, H., Cuvelier, C., Duncan, B. N., Folberth, G., Horowitz, L. W., Jonson, J., Kaminski, J. W., Marmer, E., Park, R., Pringle, K. J., Schroeder, S., Szopa, S.,
850   Takemura, T., Zeng, G., Keating, T. J., and Zuber, A.: A multi-model assessment of pollution transport to the Arctic, Atmos. Chem. Phys., 8, 5353–5372, https://doi.org/10.5194/acp-8-5353-2008, 2008.

Sierau, B., Chang, R. Y.-W., Leck, C., Paatero, J., and Lohmann, U.: Single-particle characterization of the high-Arctic summertime aerosol, Atmos. Chem. Phys., 14, 7409–7430, https://doi.org/10.5194/acp-14-7409-2014, 2014.

Silva, P. J. and Prather, K. A.: Interpretation of Mass Spectra from Organic Compounds in Aerosol Time-of-Flight Mass Spectrometry, Anal.
855   Chem., 72, 3553–3562, https://doi.org/10.1021/ac9910132, 2000.

Silva, P. J., Liu, D.-Y., Noble, C. A., and Prather, K. A.: Size and Chemical Characterization of Individual Particles Resulting from Biomass Burning of Local Southern California Species, Environ. Sci. Technol., 33, 3068–3076, https://doi.org/10.1021/es980544p, 1999.

Singh, H. B., Anderson, B. E., Brune, W. H., Cai, C., Cohen, R. C., Crawford, J. H., Cubison, M. J., Czech, E. P., Emmons, L., Fuelberg, H. E., Huey, G., Jacob, D. J., Jimenez, J. L., Kaduwela, A., Kondo, Y., Mao, J., Olson, J. R., Sachse, G. W., Vay, S. A., Weinheimer, A.,
860   Wennberg, P. O., and Wisthaler, A.: Pollution influences on atmospheric composition and chemistry at high northern latitudes: Boreal and California forest fire emissions, Atmos. Environ., 44, 4553–4564, http://www.sciencedirect.com/science/article/pii/S1352231010007004, 2010.

Sobhani, N., Kulkarni, S., and Carmichael, G. R.: Source sector and region contributions to black carbon and $PM_{2.5}$ in the Arctic, Atmos. Chem. Phys., 18, 18 123–18 148, https://doi.org/10.5194/acp-18-18123-2018, 2018.

865 Spencer, M. T., Holecek, J. C., Corrigan, C. E., Ramanathan, V., and Prather, K. A.: Size-resolved chemical composition of aerosol particles during a monsoonal transition period over the Indian Ocean, J. Geophys. Res.-Atmos., 113, https://doi.org/10.1029/2007JD008657, 2008.

Stohl, A.: Computation, accuracy and applications of trajectories: A review and bibliography, Atmos. Environ., 32, 947 – 966, http://dx.doi. org/10.1016/S1352-2310(97)00457-3, 1998.

Stohl, A.: Characteristics of atmospheric transport into the Arctic troposphere, J. Geophys. Res.-Atmos., 111,
870   https://doi.org/10.1029/2005JD006888, 2006.

Stohl, A., Forster, C., Eckhardt, S., Spichtinger, N., Huntrieser, H., Heland, J., Schlager, H., Wilhelm, S., Arnold, F., and Cooper, O.: A backward modeling study of intercontinental pollution transport using aircraft measurements, J. Geophys. Res.-Atmos., 108, https://doi.org/10.1029/2002JD002862, 2003.

Stohl, A., Forster, C., Frank, A., Seibert, P., and Wotawa, G.: Technical note: The Lagrangian particle dispersion model FLEXPART version
875   6.2, Atmos. Chem. Phys., 5, 2461–2474, https://doi.org/10.5194/acp-5-2461-2005, 2005.

Stohl, A., Klimont, Z., Eckhardt, S., Kupiainen, K., Shevchenko, V. P., Kopeikin, V. M., and Novigatsky, A. N.: Black carbon in the Arctic: the underestimated role of gas flaring and residential combustion emissions, Atmos. Chem. Phys., 13, 8833–8855, https://doi.org/10.5194/acp-13-8833-2013, 2013.

Stroeve, J. C., Serreze, M. C., Holland, M. M., Kay, J. E., Malanik, J., and Barrett, A. P.: The Arctic's rapidly shrinking sea ice cover: a research synthesis, Climatic Change, 110, 1005–1027, https://doi.org/10.1007/s10584-011-0101-1, 2012.

Stull, R. B.: An Introduction to Boundary Layer Meteorology, Kluwer Academic Publishers, https://doi.org/10.1007/978-94-009-3027-8, 1997.

Sullivan, R. C. and Prather, K. A.: Recent Advances in Our Understanding of Atmospheric Chemistry and Climate Made Possible by On-Line Aerosol Analysis Instrumentation, Anal. Chem., 77, 3861–3886, https://doi.org/10.1021/ac050716i, 2005.

Sullivan, R. C. and Prather, K. A.: Investigations of the Diurnal Cycle and Mixing State of Oxalic Acid in Individual Particles in Asian Aerosol Outflow, Environ. Sci. Technol., 41, 8062–8069, https://doi.org/10.1021/es071134g, 2007.

Thomson, D. S., Middlebrook, A. M., and Murphy, D. M.: Thresholds for Laser-Induced Ion Formation from Aerosols in a Vacuum Using Ultraviolet and Vacuum-Ultraviolet Laser Wavelengths, Aerosol Sci. Technol., 26, 544–559, https://doi.org/10.1080/02786829708965452, 1997.

Tjernström, M., Birch, C. E., Brooks, I. M., Shupe, M. D., Persson, P. O. G., Sedlar, J., Mauritsen, T., Leck, C., Paatero, J., Szczodrak, M., and Wheeler, C. R.: Meteorological conditions in the central Arctic summer during the Arctic Summer Cloud Ocean Study (ASCOS), Atmos. Chem. Phys., 12, 6863–6889, https://doi.org/10.5194/acp-12-6863-2012, 2012.

Tremblay, S., Picard, J.-C., Bachelder, J. O., Lutsch, E., Strong, K., Fogal, P., Leaitch, W. R., Sharma, S., Kolonjari, F., Cox, C. J., Chang, R. Y.-W., and Hayes, P. L.: Characterization of aerosol growth events over Ellesmere Island during the summers of 2015 and 2016, Atmos. Chem. Phys., 19, 5589–5604, https://doi.org/10.5194/acp-19-5589-2019, 2019.

Wandel, M.: CO-Messung in der Arktis im Rahmen der NETCARE-Kampa-gne, Master's thesis, Johannes Gutenberg-Universität Mainz, 2015.

wetter3: http://www1.wetter3.de/archiv_gfs_dt.html, last access: July 2020, 2020.

Willis, M. D., Burkart, J., Thomas, J. L., Köllner, F., Schneider, J., Bozem, H., Hoor, P. M., Aliabadi, A. A., Schulz, H., Herber, A. B., Leaitch, W. R., and Abbatt, J. P. D.: Growth of nucleation mode particles in the summertime Arctic: a case study, Atmos. Chem. Phys., 16, 7663–7679, https://doi.org/10.5194/acp-16-7663-2016, 2016.

Willis, M. D., Köllner, F., Burkart, J., Bozem, H., Thomas, J. L., Schneider, J., Aliabadi, A. A., Hoor, P. M., Schulz, H., Herber, A. B., Leaitch, W. R., and Abbatt, J. P. D.: Evidence for marine biogenic influence on summertime Arctic aerosol, Geophys. Res. Lett., 44, 6460–6470, https://doi.org/10.1002/2017GL073359, 2017.

Willis, M. D., Leaitch, W. R., and Abbatt, J. P.: Processes Controlling the Composition and Abundance of Arctic Aerosol, Rev. Geophys., 56, 621–671, https://doi.org/10.1029/2018RG000602, 2018.

Winiger, P., Andersson, A., Eckhardt, S., Stohl, A., Semiletov, I. P., Dudarev, O. V., Charkin, A., Shakhova, N., Klimont, Z., Heyes, C., and Gustafsson, Ö.: Siberian Arctic black carbon sources constrained by model and observation, P. Natl. Acad. Sci., 114, E1054–E1061, https://doi.org/10.1073/pnas.1613401114, 2017.

Xu, J.-W., Martin, R. V., Morrow, A., Sharma, S., Huang, L., Leaitch, W. R., Burkart, J., Schulz, H., Zanatta, M., Willis, M. D., Henze, D. K., Lee, C. J., Herber, A. B., and Abbatt, J. P. D.: Source attribution of Arctic black carbon constrained by aircraft and surface measurements, Atmos. Chem. Phys., 17, 11 971–11 989, https://doi.org/10.5194/acp-17-11971-2017, 2017.

Yang, F., Chen, H., Wang, X., Yang, X., Du, J., and Chen, J.: Single particle mass spectrometry of oxalic acid in ambient aerosols in Shanghai: Mixing state and formation mechanism, Atmos. Environ., 43, 3876 – 3882, https://doi.org/10.1016/j.atmosenv.2009.05.002, 2009.

915 Yang, Y., Wang, H., Smith, S. J., Easter, R. C., and Rasch, P. J.: Sulfate Aerosol in the Arctic: Source Attribution and Radiative Forcing, J. Geophys. Res.-Atmos., 123, 1899–1918, https://doi.org/10.1002/2017JD027298, 2018.

Zauscher, M. D., Wang, Y., Moore, M. J. K., Gaston, C. J., and Prather, K. A.: Air Quality Impact and Physicochemical Aging of Biomass Burning Aerosols during the 2007 San Diego Wildfires, Environ. Sci. Technol., 47, 7633–7643, https://doi.org/10.1021/es4004137, 2013.

Zhang, X., Smith, K. A., Worsnop, D. R., Jimenez, J. L., Jayne, J. T., Kolb, C. E., Morris, J., and Davidovits, P.: Numerical Char-

920 acterization of Particle Beam Collimation: Part II Integrated Aerodynamic-Lens-Nozzle System, Aerosol Sci. Technol., 38, 619–638, https://doi.org/10.1080/02786820490479833, 2004.

Zhu, C., Kanaya, Y., Takigawa, M., Ikeda, K., Tanimoto, H., Taketani, F., Miyakawa, T., Kobayashi, H., and Pisso, I.: FLEXPART v10.1 simulation of source contributions to Arctic black carbon, Atmospheric Chemistry and Physics, 20, 1641–1656, https://doi.org/10.5194/acp-20-1641-2020, https://www.atmos-chem-phys.net/20/1641/2020/, 2020.